demonstrated erosive arthritis with many features resembling those of RA.

Materials and Methods

Ethics Statement and Preparation of humanized mice

NOG mice were obtained from the Central Institute for Experimental Animals (Kawasaki, Japan), and protocols for experiments with NOG mice were approved by the Institutional Animal Care and Use Committee of the National Institute of Infectious Diseases (NIID; Tokyo, Japan) (certification number 206061, 14th. April 2006). Cord blood was obtained from the Tokyo Cord Blood Bank (Tokyo, Japan) after acquiring informed consent from the parents of the donors. Protocols for experiments with human materials were approved by the Institutional Review Boards of the National Research Institute for Child Health and Development (Tokyo, Japan) (certification number 139, 22th. March 2005), the NIID (certification number 1, 17th. October 1997), and the Tokyo Cord Blood Bank (certification number 06-17-02, 18th. August 2006). Isolation of human $CD34^+$ HSCs from cord blood using the MACS Direct CD34 Progenitor Cell Isolation Kit (Miltenyi Biotec, Bergisch Gladbach, Germany), their intravenous injection (1×10^4 to 1.2×10^5 cells/mouse) into 6- to 10-week-old female NOG mice, and characterization of reconstitution of human hematoimmune system components in these mice were performed as described elsewhere[17]. NOG mice were not irradiated prior to transplantation with $CD34^+$ HSCs, because they lived significantly longer after humanization and satisfactory development of human immune system components were observed without irradiation [18]. NOG mice in which human hematoimmune system components were reconstituted are referred to here as humanized NOG (hNOG) mice.

Analysis on the reconstitution of human lymphoid system components in hNOG mice

Peripheral blood mononuclear cells were isolated weekly from NOG mice following transplantion with human $CD34^+$ stem cells and examined for the reactivity with the following antibodies by flow cytometry: FITC-conjugated anti–human CD45 (J.33), CD3 (UCHT1), CD4 (13B8.2), CD19 (J4.119), and CD45RO (UCHL1) (all from Beckman Coulter, Brea, CA); PE-conjugated anti–human CD4 (13B8.2), CD8 (B9.11), CD19 (J4.119), CD45RA (ALB11) (all from Beckman Coulter), and CXCR4 (44717; R&D Systems, Minneapolis, MN); anti–mouse CD45 (YW62.3; Beckman Coulter); ECD-conjugated anti–human CD45 (J.33; Beckman Coulter); and PC5-conjugated anti–human CD8 (T8) and CD14 (Rm052) (all from Beckman Coulter). Flow cytometric analysis was conducted by 2- or 4-color staining using the EpicsXL flow cytometer (Beckman Coulter).

Experimental EBV infection and quantification of viral DNA

Supernatant fluid of Akata cell culture was prepared as described previously[15] and used as EBV inoculum. EBV dose in 50% transformation dose (TD_{50}) was determined by a standard method as described previously[15]. EBV was inoculated intravenously through the tail vein. Peripheral blood EBV DNA load was quantified by real-time polymerase chain reaction (PCR) based on the TaqMan system (Applied Biosystems), as described elsewhere[19]. As a control, nine hNOG mice were left uninfected; among them four mice were inoculated with supernatant fluid of EBV-negative Akata cell culture.

Histopathology, in situ hybridization (ISH), and immunohistochemistry

hNOG mice were sacrificed 1 to 12 months after inoculation with EBV and their major joints including knees and ankles were removed and fixed in 10% formalin solution. These specimens were embedded in paraffin and stained with hematoxylin-eosin (HE) for histological examinations. For phenotypic analysis of proliferating lymphocytes, immunostaining with the antibodies specific to human CD3 (DAKO, A0452), CD4 (Leica, NCL-CD4-1F6), CD8 (Leica, NCL-CD8-4B11), CD20 (DAKO, M0755) and CD68 (DAKO, M0876) was performed on paraffin sections. EBV was detected by in-situ hybridization (ISH) with EBV-encoded small RNA (EBER) probes (DAKO, Y5200).

Statistical Analysis

Fisher's exact test was used for categorical data. Analyses were performed using JMP 7.0.2 for Windows (SAS Institute Inc., Cary, NC). All tests were two-tailed, with differences reported as significant when p values were less than 0.01.

Results

Twenty-three hNOG mice, prepared with $CD34^+$ cells isolated from ten different cord blood samples and inoculated with EBV were examined histopathologically for the presence of erosive arthritis. The number of transplanted $CD34^+$ cells ($0.1–1.2\times10^5$ cells), days from transplantation with $CD34^+$ cells to inoculation with EBV (106–197 days), dose of EBV inoculated ($10^0–10^3$ TD_{50}), days from EBV inoculation to autopsy (26–320 days) for each mouse are described in Table S1. As a control, nine hNOG mice prepared with $CD34^+$ cells isolated from three different cord blood samples and not inoculated with EBV were examined similarly (Table S1). Among them, four mice were mock inoculated with culture supernatant of EBV-negative Akata cells. HE staining of major joints including knees and ankles revealed synovial proliferation and infiltration of inflammatory cells in the synovium in 15 of the 23 EBV-infected hNOG mice (65%), whereas none of the nine control hNOG mice showed these signs of arthritis ($P = 0.001$ by the two-tailed Fisher's exact test) (Fig. 1A and Table 1). Development of arthritis was not dependent on viral dose, because hNOG mice developed arthritis following EBV inoculation at each dose (10^0, 10^1, 10^2, 10^3 TD_{50}) (Table S1). The earliest time point when arthritis was observed was 26 days post-infection and it was seen as late as 320 days post-infection. In a fraction of examined mice, granulation tissue overgrew the bearing surface of the joint and was associated with the breakdown of the articular surface. Furthermore, multinuclear giant cells similar to osteoclasts were seen in the granulation tissue that invaded the bone on the joint edge (Figure 1A). This histology is remarkably similar to the pannus formation seen in erosive arthritis characteristic to RA. In the bone marrow adjacent to inflamed joints, infiltration of activated mononuclear cells generated a histology reminiscent of bone marrow edema characteristic to RA (Fig. 1A).

Immunostaining with monoclonal antibodies revealed a large number of CD3-positive T cells among the proliferating cells in the synovial tissue (Fig. 1B). Both $CD4^+$ and $CD8^+$ cells were identified. There were also a few $CD20^+$ B cells and $CD68^+$ macrophages. When the bone marrow adjacent to inflamed joint tissue was examined by immunostaining, CD3-positive cells and CD4-positive cells were detected, while almost no cells exhibited positive CD20 staining (Figure 1B). It should be noted that because NOG mice lack T, B, and NK lymphocytes completely and human-specific antibodies were used here, all lymphocytes detected in hNOG mouse tissues are considered to be of human origin. EBER ISH revealed only few EBV-infected

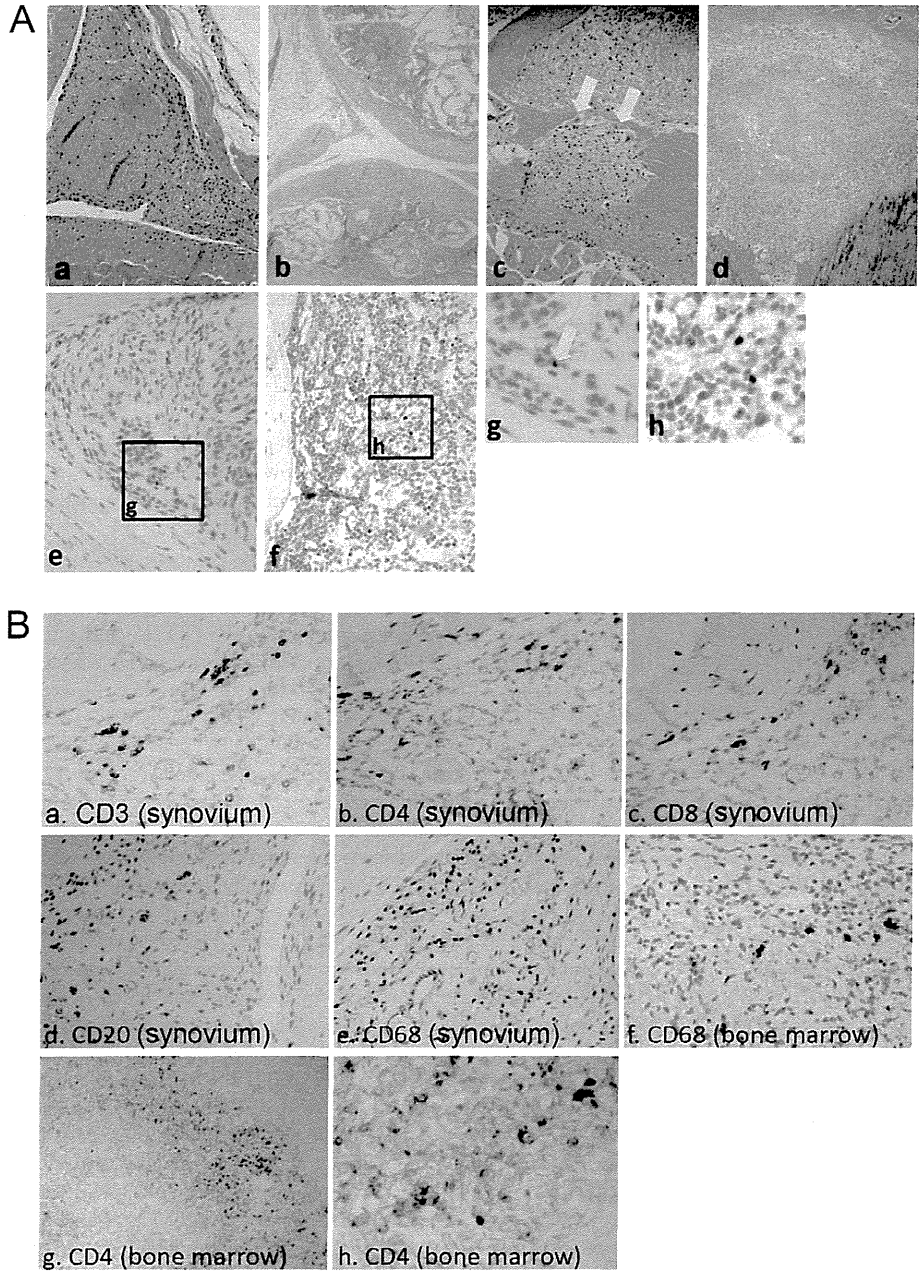

Figure 1. Histopathology of joint and adjacent bone marrow tissues in hNOG mice infected with EBV. A. HE staining and EBER ISH. HE staining of a knee joint in the EBV-infected mouse N70-13 (Table S1), showing synovial proliferation (a): a knee joint in the control mouse N69-1 not infected with EBV (b): a knee joint in the EBV-infected mouse N87-6 (Table S1), showing a pannus-like lesion containing multinuclear giant cells (yellow arrows) (c): and bone marrow near the knee joint of N70-13, showing edema (d). EBER ISH in the synovium of a knee joint in the EBV-infected mouse N79-1 (Table S1), showing few EBV-infected cells (e), and in the bone marrow adjacent to the affected knee joint of the same mouse, demonstrating a number of EBV-infected cells (f). g and h represent further magnification of a portion of e and f, respectively. The yellow arrow indicates an $EBER^+$ cell. Original magnification, ×200 (a, c, d, e, f), ×100 (b). B. Immunostaining. Joint (a–e) and adjacent bone marrow tissues (f–h) from the N70-13 mouse were examined for the expression of CD3 (a), CD4 (b, g, h), CD8 (c), CD20 (d), and CD68 (e, f). Original magnification; x200 (a–b), x400 (c–f), x100 (g), x400 (h).
doi:10.1371/journal.pone.0026630.g001

cells in the synovial membrane of affected joints (Fig. 1A), whereas numerous EBV-infected cells were detected in the bone marrow near the affected joints (Fig. 1A).

Discussion

Erosive arthritis was observed in 15 among the 23 hNOG mice infected with EBV but not in nine control mice that were reconstituted with human immune system components but not inoculated with EBV. The incidence of erosive arthritis is significantly elevated among EBV-infected mice compared with control uninfected mice ($P = 0.001$ by the two-tailed Fisher's exact test). This erosive arthritis is accompanied by pannus formation, synovial membrane proliferation, inflammatory cell infiltration to the synovium, and bone marrow edema, rendering it closely similar to the tissue of RA. In addition, numerous EBER-positive

Table 1. Development of arthritis in EBV-infected hNOG mice.

Arthritis	EBV-infected	Un-infected
(+)	15 *	0
(−)	8	9

*p = 0.001, by two-tailed Fisher's exact test.
doi:10.1371/journal.pone.0026630.t001

cells were seen in the edematous bone marrow adjacent to the affected joint. Thus, these results provide the first evidence that EBV can induce erosive arthritis resembling RA in experimental animals. We examined whether anti-cyclic citrullinated peptide (CCP) antibodies and rheumatoid factor (RF), two major markers of RA, were present in the blood of hNOG, but neither was detected.

Few EBER-positive cells were detected in the synovium of affected mouse joints and therefore it is unlikely that EBV-infected cells elicited strong virus-specific immune responses in the synovium and these immune responses triggered aberrant effects damaging the surrounding tissue. However, as numerous $CD4^+$ T cells, as well as $EBER^+$ cells, were found in the edematous bone marrow adjacent to the affected joint, it is conceivable that migration of inflammatory cells from bone marrow to synovium via ostioles, as Ochi an others suggested, had a role in the initiation of erosive arthritis [20]. It is also possible that inflammatory cytokines produced in bone marrow diffused through the nutrient canal or the nutrient foramen to the synovium and induce the proliferation of synoviocytes and the activation of osteoclasts in the adjacent joint. Significant levels (150–200 pg/ml) of IFN-γ were detected in the plasma of EBV-infected humanized mice. Antigenic cross reaction between EBV proteins and host mouse tissues might have been also involved in the pathogenesis of erosive arthritis in the mice. It should be noted, however, that after rigorous examination we have not detected anti-EBV antibodies in EBV-infected hNOG mice, except for anti-$p18^{BFRF3}$ (the18-kDa protein encoded by the third rightward open reading frame in the BamHI F fragment) IgM antibody shown in four out of thirty examined mice[15]. We did not detect antibodies to either EBNA1 that cross-reacts with a 62 kDa protein found in the synovium affected by RA [5] or gp110 that cross-reacts with HLA-DR [6,21]. Antigenic mimicry involving humoral immune responses may thus be unlikely to have a major role in the pathogenesis of erosive arthritis in hNOG mice. In contrast, we observed abundant T-cell response to EBV infection in hNOG mice[15,16] and it is conceivable that these strong T-cell response has some role in the generation of erosive arthritis.

The present mouse model of erosive arthritis may be an excellent system to investigate the pathogenesis of RA. In this model, it is feasible to remove particular cellular or molecular factors implicated in the pathogenesis of RA by administration of specific antibodies or specific functional antagonists[16]. Analysis on the effects of these antibodies or antagonists will clarify the role of individual cellular and molecular components of the immune system and hence give new insights to the pathogenesis of RA. In a similar approach, this model can also be used to search for molecular and/or cellular targets of novel therapeutics for RA.

Supporting Information

Table S1 hNOG mice examined for the development of arthritis.
(DOC)

Acknowledgments

We thank Ms. Eiko Ishizuka and Mr. Hiroyuki Masuda for their excellent technical assistance.

Author Contributions

Conceived and designed the experiments: MT SF. Performed the experiments: YK MY K-II TN NK MS NS NY NI. Analyzed the data: MS HS NS NY SS MT YK MY SF JT. Wrote the paper: MT YK HI. Mainly wrote the manuscript: MT YK. Corrected the grammar and spelling of the manuscript: HI. Supervised the project: MT. Produced and provided NOG mice: MI. Performed the computational and statistical data analyses: YK HI.

References

1. Alspaugh MA, Jensen FC, Rabin H, Tan EM (1978) Lymphocytes transformed by Epstein-Barr virus. Induction of nuclear antigen reactive with antibody in rheumatoid arthritis. J Exp Med 147: 1018–1027.
2. Billings PB, Hoch SO, White PJ, Carson DA, Vaughan JH (1983) Antibodies to the Epstein-Barr virus nuclear antigen and to rheumatoid arthritis nuclear antigen identify the same polypeptide. Proc Natl Acad Sci U S A 80: 7104–7108.
3. Rhodes G, Carson DA, Valbracht J, Houghten R, Vaughan JH (1985) Human immune responses to synthetic peptides from the Epstein-Barr nuclear antigen. J Immunol 134: 211–216.
4. Rumpold H, Rhodes GH, Bloch PL, Carson DA, Vaughan JH (1987) The glycine-alanine repeating region is the major epitope of the Epstein-Barr nuclear antigen-1 (EBNA-1). J Immunol 138: 593–599.
5. Fox R, Sportsman R, Rhodes G, Luka J, Pearson G, et al. (1986) Rheumatoid arthritis synovial membrane contains a 62,000-molecular-weight protein that shares an antigenic epitope with the Epstein-Barr virus-encoded associated nuclear antigen. J Clin Invest 77: 1539–1547.
6. Roudier J, Rhodes G, Petersen J, Vaughan JH, Carson DA (1988) The Epstein-Barr virus glycoprotein gp110, a molecular link between HLA DR4, HLA DR1, and rheumatoid arthritis. Scand J Immunol 27: 367–371.
7. Takei M, Mitamura K, Fujiwara S, Horie T, Ryu J, et al. (1997) Detection of Epstein-Barr virus-encoded small RNA 1 and latent membrane protein 1 in synovial lining cells from rheumatoid arthritis patients. Int Immunol 9: 739–743.
8. Balandraud N, Meynard JB, Auger I, Sovran H, Mugnier B, et al. (2003) Epstein-Barr virus load in the peripheral blood of patients with rheumatoid arthritis: accurate quantification using real-time polymerase chain reaction. Arthritis Rheum 48: 1223–1228.
9. Lunemann JD, Frey O, Eidner T, Baier M, Roberts S, et al. (2008) Increased frequency of EBV-specific effector memory CD8+ T cells correlates with higher viral load in rheumatoid arthritis. J Immunol 181: 991–1000.
10. Scotet E, David-Ameline J, Peyrat MA, Moreau-Aubry A, Pinczon D, et al. (1996) T cell response to Epstein-Barr virus transactivators in chronic rheumatoid arthritis. J Exp Med 184: 1791–1800.
11. Tosato G, Steinberg AD, Blaese RM (1981) Defective EBV-specific suppressor T-cell function in rheumatoid arthritis. N Engl J Med 305: 1238–1243.
12. Tosato G, Steinberg AD, Yarchoan R, Heilman CA, Pike SE, et al. (1984) Abnormally elevated frequency of Epstein-Barr virus-infected B cells in the blood of patients with rheumatoid arthritis. J Clin Invest 73: 1789–1795.
13. Filipovich AH, Zhang K, Snow AL, Marsh RA (2010) X-linked lymphoproliferative syndromes: brothers or distant cousins? Blood 116: 3398–3408.
14. Takei M, Ishiwata T, Mitamura K, Fujiwara S, Sasaki K, et al. (2001) Decreased expression of signaling lymphocytic-activation molecule-associated protein (SAP) transcripts in T cells from patients with rheumatoid arthritis. Int Immunol 13: 559–565.
15. Yajima M, Imadome K, Nakagawa A, Watanabe S, Terashima K, et al. (2008) A new humanized mouse model of Epstein-Barr virus infection that reproduces persistent infection, lymphoproliferative disorder, and cell-mediated and humoral immune responses. J Infect Dis 198: 673–682.
16. Yajima M, Imadome K, Nakagawa A, Watanabe S, Terashima K, et al. (2009) T cell-mediated control of Epstein-Barr virus infection in humanized mice. J Infect Dis 200: 1611–1615.
17. Watanabe S, Terashima K, Ohta S, Horibata S, Yajima M, et al. (2007) Hematopoietic stem cell-engrafted NOD/SCID/IL2Rgamma null mice develop

human lymphoid systems and induce long-lasting HIV-1 infection with specific humoral immune responses. Blood 109: 212–218.
18. Watanabe S, Ohta S, Yajima M, Terashima K, Ito M, et al. (2007) Humanized NOD/SCID/IL2Rgamma(null) mice transplanted with hematopoietic stem cells under nonmyeloablative conditions show prolonged life spans and allow detailed analysis of human immunodeficiency virus type 1 pathogenesis. J Virol 81: 13259–13264.
19. Kimura H, Morita M, Yabuta Y, Kuzushima K, Kato K, et al. (1999) Quantitative analysis of Epstein-Barr virus load by using a real-time PCR assay. J Clin Microbiol 37: 132–136.
20. Ochi T, Hakomori S, Adachi M, Owaki H, Okamura M, et al. (1988) The presence of a myeloid cell population showing strong reactivity with monoclonal antibody directed to difucosyl type 2 chain in epiphyseal bone marrow adjacent to joints affected with rheumatoid arthritis (RA) and its absence in the corresponding normal and non-RA bone marrow. J Rheumatol 15: 1609–1615.
21. Roudier J, Petersen J, Rhodes GH, Luka J, Carson DA (1989) Susceptibility to rheumatoid arthritis maps to a T-cell epitope shared by the HLA-Dw4 DR beta-1 chain and the Epstein-Barr virus glycoprotein gp110. Proc Natl Acad Sci U S A 86: 5104–5108.

Epstein-Barr Virus BART9 miRNA Modulates LMP1 Levels and Affects Growth Rate of Nasal NK T Cell Lymphomas

Rajesh Ramakrishnan[1], Hart Donahue[1], David Garcia[1], Jie Tan[1], Norio Shimizu[2], Andrew P. Rice[1], Paul D. Ling[1]*

1 Department of Molecular Virology & Microbiology, Baylor College of Medicine, Houston, Texas, United States of America, **2** Department of Virology, Division of Virology & Immunology, Medical Research Institute, Tokyo Medical and Dental University, Tokyo, Japan

Abstract

Nasal NK/T cell lymphomas (NKTCL) are a subset of aggressive Epstein-Barr virus (EBV)-associated non-Hodgkin's lymphomas. The role of EBV in pathogenesis of NKTCL is not clear. Intriguingly, EBV encodes more than 40 microRNAs (miRNA) that are differentially expressed and largely conserved in lymphocryptoviruses. While miRNAs play a critical role in the pathogenesis of cancer, especially lymphomas, the expression and function of EBV transcribed miRNAs in NKTCL are not known. To examine the role of EBV miRNAs in NKTCL, we used microarray profiling and qRT-PCR to identify and validate expression of viral miRNAs in SNK6 and SNT16 cells, which are two independently derived NKTCL cell lines that maintain the type II EBV latency program. All EBV BART miRNAs except BHRF-derived miRNAs were expressed and some of these miRNAs are expressed at higher levels than in nasopharyngeal carcinomas. Modulating the expression of BART9 with antisense RNAs consistently reduced SNK6 and SNT16 proliferation, while antisense RNAs to BARTs-7 and -17-5p affected proliferation only in SNK6 cells. Furthermore, the EBV LMP-1 oncoprotein and transcript levels were repressed when an inhibitor of BART9 miRNA was transfected into SNK6 cells, and overexpression of BART9 miRNA increased LMP-1 protein and mRNA expression. Our data indicate that BART9 is involved in NKTCL proliferation, and one of its mechanisms of action appears to be regulating LMP-1 levels. Our findings may have direct application for improving NKTCL diagnosis and for developing possible novel treatment approaches for this tumor, for which current chemotherapeutic drugs have limited effectiveness.

Citation: Ramakrishnan R, Donahue H, Garcia D, Tan J, Shimizu N, et al. (2011) Epstein-Barr Virus BART9 miRNA Modulates LMP1 Levels and Affects Growth Rate of Nasal NK T Cell Lymphomas. PLoS ONE 6(11): e27271. doi:10.1371/journal.pone.0027271

Editor: Maria G. Masucci, Karolinska Institutet, Sweden

Received September 2, 2011; **Accepted** October 13, 2011; **Published** November 10, 2011

Funding: This project was supported in part by the Baylor–UT Houston Center for AIDS Research Core Support Grant number AI036211 from the National Institute of Allergy and Infectious Diseases to APR and PDL. RR was supported by NIH grant T32AI7456. No additional external funding received for this study. The funders had no role in study design, data collection and analysis, decision to publish, or preparation of the manuscript.

Competing Interests: The authors have declared that no competing interests exist.

* E-mail: pling@bcm.edu

Introduction

EBV is a member of the herpes virus family and is a pre-eminent human oncogenic virus with a causal relationship to several malignancies, including endemic Burkitt's lymphoma (eBL), nasopharyngeal carcinoma (NPC), a proportion of gastric carcinomas (GC), NKT-cell lymphomas (NKTCL), Hodgkin disease (HD), post-transplant lymphoma-like disease (PTLD), and leiomyosarcomas [1,2]. Within the context of AIDS, EBV is associated with a proportion of non-Hodgkin lymphomas, almost all HD, and leiomyosarcomas. The EBV genome contains over 170,000 bp encoding more than 80 genes. EBV gene expression during latency and tumorgenesis consists of distinct combinations of six nuclear proteins (EBNAs), three membrane proteins (LMPs) and multiple noncoding RNAs, including over 40 miRNAs [3,4,5,6,7]. While the EBV latent proteins have been investigated intensively for some time, the contribution of EBV-encoded miRNAs or altered cellular miRNA expression in EBV-induced cancers has not been fully explored.

The EBV miRNAs were the first viral encoded miRNAs discovered [6]. MiRNAs are ~22 nt transcripts that form imperfect duplexes with target mRNAs and thereby inhibit their expression. MiRNAs typically target the 3′ UTR of mRNAs and the average magnitude of repression of the encoded protein is ~30% [8]. EBV miRNAs are primarily derived from a group of alternatively spiced RNAs transcribed from the BamH1A region of the genome (BamA rightward transcripts or BARTs) [3,4,5,6]. The BARTs encode a large number of miRNAs and with the exception of mir-BART2; the majority are derived from two clusters. A cluster of 3 miRNAs has also been identified which are derived from the BHRF1 gene. The sum total of at least 40 EBV-encoded miRNAs dramatically increases the complexity of potentially biologically active molecules encoded by EBV during latent infection [9]. Like many of the miRNAs discovered to date, the functions of the EBV-encoded miRNAs remain poorly understood. It has been hypothesized that herpesvirus miRNAs, including those encoded by EBV, Cytomegalovirus (CMV), and Kaposi's sarcoma- associated Herpesvirus (KHSV), may facilitate the viral life cycle by blocking innate or adaptive immune responses or by interfering with the appropriate regulation of apoptosis, cell growth, or DNA replication in infected cells [9]. Herpesvirus miRNAs might also target mRNAs for viral genes that regulate the productive lytic cycle, thus having a role in maintaining latency or modulating productive lytic infection. EBV-encoded miRNAs can target both viral and cellular genes. EBV mir-BART2 targets the EBV DNA polymerase mRNA for degradation [10], which inhibits lytic replication and miRNAs from BART cluster 1 may target the viral LMP-1 protein [11]. In

addition, mir-BART5 targets the pro-apoptotic factor PUMA and mir-BHRF1-3 targets the chemokine/T-cell attractant CXCL11 [12,13]. Dysregulation of cellular miRNAs following B cell infection has also been described [11,14,15,16,17]. The cellular miRNAs 146a and 155 regulate lymphocyte signaling and gene expression pathways in this context.

Three general patterns of viral gene expression have been identified in EBV-associated cancers [1,2]. Latency I is characterized by expression of EBNA-1, while latency II is characterized by expression of EBNA-1 along with LMP1 and 2. Latency III is characterized by expression of all EBNAs and LMPs and is typically associated with B cells infected with EBV in vitro or in lymphomas in the immunosuppressed. EBV miRNAs are expressed in all EBV infected tumor cells, although they are differentially expressed in some tumors [3,4,5,6,7,18,19,20,21]. The context in which miRNA functions are investigated may be particularly important since the ubiquitous and powerful activities of all the latent proteins expressed in latency III could mask some of the activities contributed by miRNAs. Recently, several cell lines have been isolated from EBV-associated NKT cell lymphomas, which appear to select for latency II in both primary tumor tissues as well as the cell lines [22,23]. Thus, NKTCL cell lines may be a powerful model system to investigate the functions of EBV gene products within the context of latency II and may lead to insights into miRNA functions in EBV-associated HD, GC, and NPC, for which few practical cell culture systems are available.

Nasal NK/T cell lymphomas (NKTCL) are a heterogeneous group of tumors, so named because some tumors have an NK phenotype ($CD3^-$, $CD56^+$) and some have a T cell phenotype (usually $CD4^+/CD3^+$, but sometimes $CD8^+$ $CD3^+$ and sometimes $CD3^+$ 4^-, 8^- gamma delta) [24,25]. NKTCL is a distinct clinical entity characterized by necrotic lesions in the nasal cavity, nasopharynx, and palate. These are generally aggressive tumors with poor prognosis [24,25]. A universal feature of these tumors is the consistent and strong association with EBV, although the precise role of the virus in this disease remains poorly understood. Analysis of primary tumor tissue has shown a latency II pattern of EBV gene expression [22,23]. At least 7 cell lines of both NK and T cell-like phenotypes have been derived from primary tumors. These include NK-like ($CD3^-$, $CD56^+$) SNK1, -6, -10 and T-cell-like ($CD3^+$, $CD56^+$, $TCR\gamma/\delta^+$) SNT 8, -13, 15, -16 cell lines [22,23]. The cell lines, like the primary tumor tissues from which they were derived, retain latency II EBV expression patterns and the EBV genome is clonal. EBV expresses more than 40 miRNAs, but which ones are expressed in NKTCL remains unknown. We hypothesized that specific viral and cellular miRNAs are likely to play a role in the genesis and maintenance of NKTCL. To address this, we utilized microarrays and quantitative PCR to identify EBV miRNAs that are expressed in established NKTCL cell lines. Transfection of antisense oligonucleotides to some of the abundantly expressed EBV miRNAs revealed that at least one of them, BART9, contributes significantly to NKTCL proliferation. The results provide new information about the expression pattern of EBV encoded miRNAs in NKTCLs and identified a novel function for the EBV-encoded BART9 miRNA.

Results

NKTCL stably maintain the EBV Type II latency program

In tumors, EBV displays latency programs characterized by specific patterns of viral gene expression. In Burkitt's lymphoma, Type I latency is seen while Type II latency is observed in nasopharyngeal carcinoma, gastric carcinoma, and Hodgkin's disease. Type III latency is often restricted to B lymphomas in immunodeficient patients [26]. Although previous studies have found that NKTCLs have a type II latency phenotype, it is common for some EBV positive cell lines to drift towards type III latency in culture. To confirm the latency phenotype under our culture conditions, we tested five NKTCL cell lines for latent and lytic gene expression. We found that the two SNK (SNK6 and SNK10) and three SNT (SNT8, SNT15 and SNT16) cell lines expressed EBNA1 and LMP1 (Figure 1A). These cell lines did not express the other EBNA proteins, EBNA-LP, EBNA3C and EBNA2 (Figure 1B). We also found that there was no expression of

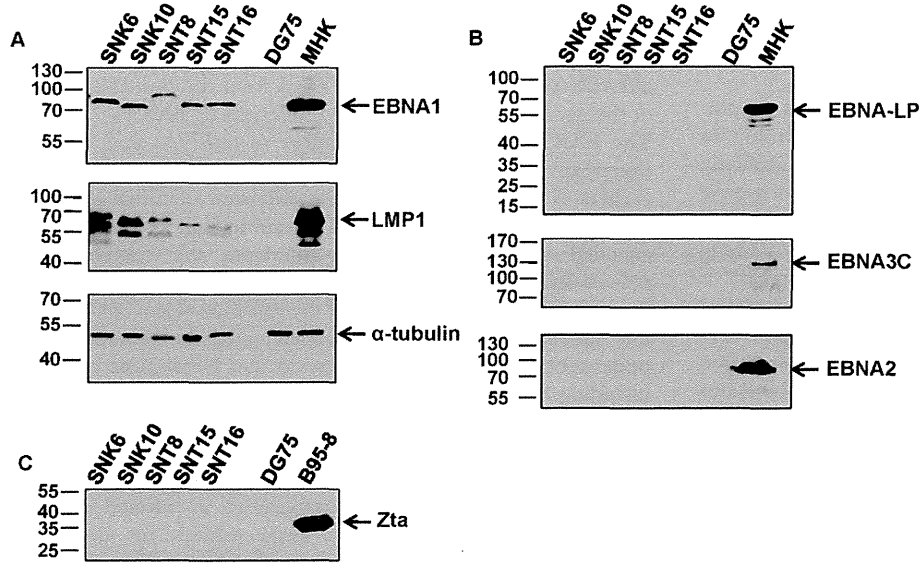

Figure 1. Characterization of NK T cell lymphoma cell lines by immunoblot analysis. Cell lysates were prepared from two NK-like (SNK6, SNK10) and three T cell-like (SNT8, SNT15 and SNT16) NKTCLs. Immunoblots were performed to analyze the expression of the indicated EBV latent and lytic proteins. EBV negative DG75 cells were used as a negative control and EBV positive MHK cells, which maintain Latency III gene expression and express all of the latent proteins, were used as a positive control.
doi:10.1371/journal.pone.0027271.g001

Zta lytic protein (Figure 1C). These data indicate that the NKTCL cell lines stably exhibit a Type II latency program.

miRNA microarray profiling of NKTCL

Nasal NK/T cell lymphomas (NKTCLs) have been demonstrated to be consistently associated with Epstein-Barr virus (EBV) as all cases are EBV positive [27,28,29]. EBV encodes at least 40 microRNAs (miRNA) [3] and there is increasing evidence for the role that miRNAs play in malignant transformation of cells [30]. Therefore, to investigate the role of EBV miRNAs in NKTCL oncogenesis, we first carried out miRNA microarray profiling. We isolated total RNA from two representative NKTCL cell lines, SNK6 and SNT16. Both SNK6 and SNT16 express cellular and EBV proteins that are consistent with prototypical NK and T-cell like NKTCLs respectively. These cell lines were also chosen for microarray profiling and further analysis because of their robust growth and viability in cell culture relative to other known SNK or SNT cell lines. A miRHumanVirus microarray chip was used to examine the expression levels of 1100 mature miRNAs that included human (875) and viral (225) miRNAs. The probes also included 44 EBV miRNAs in the microarray chip.

We used the criteria and statistical parameters described in the Methods to analyze the EBV miRNA expression patterns in the two NKTCL cell lines. Using a median expression value cut-off of 500, we identified 19–21 EBV miRNAs that were present at relatively high levels in SNK6 and SNT16 cell lines (Fig. 2A). To verify the reliability of the microarray data, we selected seven EBV miRNAs whose expression in the microarray ranged from high to low and carried out Taqman PCR on total RNA extracted from SNK6 and SNT16 cells. To more easily compare the relative expression levels of these miRNAs to previous studies, miRNA levels are shown normalized to either 10 pg total RNA or as copy numbers per cell. As shown in Figure 2B and C, the relative expression level of EBV miRNAs BART17-5p, BART7, BART1-3p, BART9, and BART10 was at least one log higher than EBV miRNA BART2-3p in both SNK6 and SNT16 cells. The levels of the miRNAs were also higher in SNT16 cells than SNK6 cells. This is in agreement with the microarray data which also showed a higher expression level of the selected miRNAs in SNT16 cells compared to SNK6 cells (Fig. 2B). Notably, BHRF1 derived miRNAs were nearly undetectable (Fig. 2A–C). These data indicate that the microarray profiling data are generally reliable and this analysis has therefore determined the set of EBV miRNAs which are expressed in the SNK6 and SNT16 cell lines.

Reducing EBV miRNA levels affect SNK6 and SNT16 growth rate

miRNAs regulate many genes including, those involved in cell growth [31]. We first investigated the consequences of blocking EBV miRNA function on the growth rate of SNK6 and SNT16 NKT-cell lines. Based on the miRNA microarray profile (Fig. 2), we chose six EBV miRNAs that were expressed at high levels in both cell lines. The six EBV miRNAs were individually inhibited by transfection LNA-modified antisense oligonucleotides. Samples were collected every 24 hours for three days and cell numbers and viability analyzed. The anti-EBV-miR-BART9, anti-EBV-miR-BART7 and anti-miR- BART17-5p showed a statistically significant reduction in SNK6 cell growth (~19%, ~20% and ~29%, respectively) (Fig. 3A). EBV-miR-BART1-5p and EBV-miR-BART16 antisense oligonucleotides did not have statistically significant effects on SNK6 growth rate. Also there was no significant effect on the viability of the SNK6 cells upon inhibition of any of the EBV miRNAs shown in Figure 3A (Fig. 3B). In SNT16 cells, only anti-EBV-miR-BART9 showed a statistically significant decrease (~34%) in cell growth. Anti-EBV-miR-BART16, anti-EBV-miR-BART17-5p, anti-EBV-miR-BART7, anti-EBV-miR1-5p affected cell growth by ~25%, ~3%, ~10% and ~7%, respectively, but these differences were not statistically significant in a paired t-test (Fig. 3C). We noted that there was a decrease of ~20% in viability of SNT16 cells when the levels of EBV miRNAs were reduced (data not shown). Anti-EBV-miR-BART1-3p showed an increase in SNK6 and SNT16 cell growth, but this difference was not statistically significant (Fig. 3A and C). A scrambled control miRNA had no detectable effect on proliferation or viability on either cell line (Fig. 3). This data suggests that the expression levels of some EBV miRNAs may play a role in cell proliferation.

Inhibiting EBV miR-BART9 reduces LMP1 protein and mRNA expression in SNK6 cells

Because reducing BART9 levels affected growth rate in SNK6 and SNT16 cells (Fig. 3), we focused further experiments on the BART9 miRNA. EBV-encoded LMP1 triggers multiple cellular signaling pathways that influence cell growth [32]. We carried out immunoblot analysis to investigate if the effect on growth rate upon reduction of EBV BART miRNA was a result of altered LMP1 expression. SNK6 cells were transfected with either control miRNA (Scramble) or anti-EBV-miR BART9 and cells were lysed 96 hours post-transfection. Immunoblots were performed and probed for LMP1 levels. We found that inhibiting EBV miR-BART9 reduced LMP1 protein expression by almost 50% when normalized to the Hsp70 loading control and relative to the control miRNA (Fig. 4A). In these experiments, we also probed for lytic protein Zta in order to examine if the activation of EBV lytic program was the reason for reduced SNK6 cell growth rate and found no detectable expression of Zta protein (data not shown). We also investigated the kinetics of anti-EBV-miR-BART9 effect on LMP1 level by carrying out a time-course experiment. We observed that there was a ~46% reduction of LMP1 protein level 96 hours post-transfection of anti-EBV-miR-BART9 compared to control miRNA (Fig. 4B).

We next examined if the ~50% reduction in LMP1 protein level following inhibition of BART9 was a consequence of reduced LMP1 mRNA expression. SNK6 cells were transfected with anti-EBV-miR-BART9 and total RNA extracted from the cells 96 hours post-transfection. cDNA was synthesized and Q-PCR was performed using LMP1 specific primers. We found that there was ~2-fold decrease in the LMP1 mRNA levels when BART9 was inhibited (Fig. 4C). This data suggests that BART9 miRNA functions as a positive factor for LMP1 at the level of mRNA accumulation.

EBV miR-BART9 has a positive effect on LMP1 protein and mRNA expression in SNK6 cells

If BART9 does indeed have a positive influence on LMP1 expression, then increasing its level might be predicted to increase LMP1 expression, in contrast to the effect of the antisense BART9 miRNA (Fig. 3, 4). To test this prediction, we transfected a precursor for miRNA-BART9 (pre-EBV-miR-BART9) into SNK6 cells and performed immunoblots and Q-RT-PCR to examine levels of LMP1 protein and mRNA, respectively. We found that increasing BART9 levels increased LMP1 protein expression by ~33% relative to cells transfected with the precursor negative control miRNA (pre-NegCtrl) when normalized to the loading control β-actin (Fig. 5A). We also found that over expressing BART9 increased the LMP1 mRNA level by a factor of 1.7 (Fig. 5B).

A

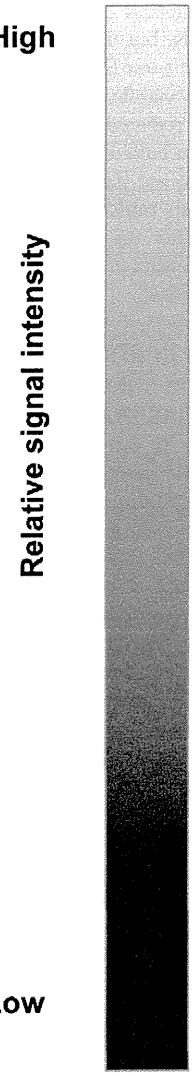

	SNK6	SNT16
ebv-miR-BART17-5p	8,343	10,472
ebv-miR-BART7	7,752	13,936
ebv-miR-BART1-3p	6,283	13,446
ebv-miR-BART9	5,951	12,277
ebv-miR-BART1-5p	5,916	10,270
ebv-miR-BART16	5,447	12,926
ebv-miR-BART14	4,681	7,458
ebv-miR-BART22	4,104	8,655
ebv-miR-BART8*	3,587	7,982
ebv-miR-BART8	3,519	8,180
ebv-miR-BART4	3,352	6,850
ebv-miR-BART19-3p	3,300	3,646
ebv-miR-BART5	2,702	4,046
ebv-miR-BART10	2,056	3,332
ebv-miR-BART12	1,953	2,623
ebv-miR-BART11-3p	1,920	2,347
ebv-miR-BART6-3p	1,834	3,152
ebv-miR-BART18-5p	1,215	4,551
ebv-miR-BART2-5p	1,074	2,122
ebv-miR-BART17-3p	458	904
ebv-miR-BART2-3p	415	1,073
ebv-miR-BART15	56	17
ebv-miR-BART20-5p	46	53
ebv-miR-BART18-3p	44	23
ebv-miR-BART10*	36	0
ebv-miR-BART20-3p	31	25
ebv-miR-BART5*	19	37
ebv-miR-BHRF1-2*	14	37
ebv-miR-BHRF1-2	10	23
ebv-miR-BHRF1-1	9	27
ebv-miR-BHRF1-3	3	16

B

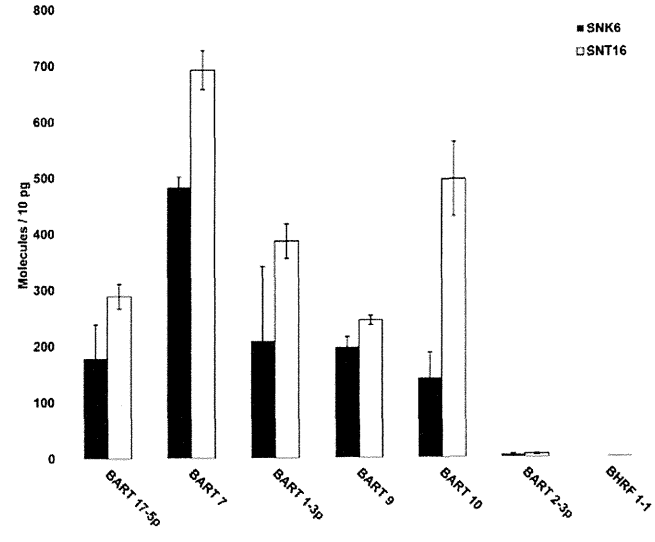

C

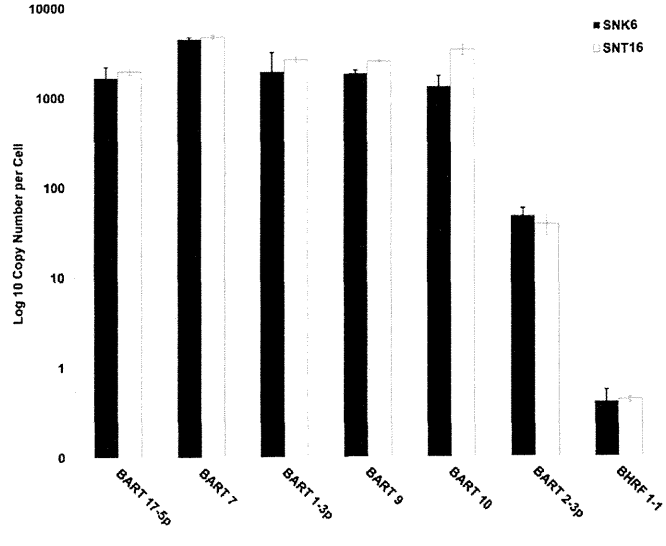

Figure 2. MiRNA expression profile in NK T cell lymphoma cell lines. (**A**) The table shows the median expression values from normalized, log-ratio (base 2) data sets of representative EBV miRNAs in SNK6 and SNT16 cell lines arranged in a descending order of expression levels. (**B**) Taqman qPCR for selected EBV miRNAs in SNK6 and SNT16 cells. The indicated EBV miRNAs were quantified using a stem-loop PCR protocol described by Chen et al [46] for detecting miRNAs. The copy number of each of the miRNAs was determined by reverse transcription and amplification of synthetic miRNAs. The graph represents miRNA expression as molecules per 10 picogram RNA. (**C**) Taqman qPCR for indicated EBV miRNAs in SNK6 and SNT16 cells as described in (B). The data are presented as copy number of EBV miRNA per cell.
doi:10.1371/journal.pone.0027271.g002

Increase in EBV-miRNA-BART9 level modestly affects SNK6 cell growth

The role of LMP1 as the oncoprotein of EBV is dependent on its expression level. While LMP1 has been reported to promote cellular transformation, increased expression of LMP1 can inhibit cell growth [33]. We next investigated whether increasing BART9 levels would inhibit SNK6 cell growth. Precursor BART9 was transfected into SNK6 cells and samples were collected every 24 hours for three days and cell numbers and viability analyzed. We found that increasing BART 9 levels modestly (~8%) affected SNK6 cell growth rate (Figure 6A) without affecting viability (Figure 6B). Although the data for reduction in growth rate of SNK6 following over-expression of BART9 did not show a statistically significant difference in a paired t-test, the results of three independent experiments showed a clear and reproducible trend of reduced growth. This suggests that the level of LMP1 needs to be regulated stringently as an increase (Figure 6) or decrease below a threshold point (Figure 3 and 4) has an inhibitory effect on SNK6 cell growth. To determine whether the effects of BART9 miRNA on LMP1 expression are directed through the 3′UTR of the LMP1 mRNA, we cotransfected a BART 9 miRNA precursor with an LMP1 expression plasmid containing the natural 3′UTR and a plasmid lacking this element in HeLa cells. Under these conditions, BART9 had no effect on LMP1 expression from either expression plasmid, suggesting that the effects of BART9 on LMP1 expression are indirect (data not shown).

Discussion

In this study we show that ~20 EBV miRNAs are abundantly expressed in Nasal NK/T cell lymphomas (NKTCL). We also provide evidence that modulating EBV miRNA levels impacts NKTCL growth rate. Furthermore, we found a direct correlation between levels of EBV-miR-BART9 and LMP1 protein and mRNA expression. Together, these observations suggest that BART9 miRNA positively modulates expression of LMP1 and one manifestation of perturbing this regulation is a retardation of NKTCL cell growth.

A number of studies have characterized EBV miRNA expression and their roles in nasopharyngeal carcinomas [4,11,19]. Other studies have focused on the role of cellular miRNAs in NKTCLs [34] and other human cancers [35]. While EBV miRNAs have been found to be conserved evolutionarily [3], they are differentially expressed in different cell types [3,7]. However, to our knowledge this is the first study to determine the expression of EBV miRNAs in NKTCLs. We found that at least 19 EBV miRNAs are abundantly expressed in NKTCLs. Indeed, these 19 miRNAs appear to be expressed at levels 2–3 logs higher than their expression in NPCs [19]. We note that a limitation of our study is that only two NKTCL cell lines and no primary tumors were profiled. Nevertheless, our data suggest that even though EBV viral gene expression might be similar to NPC and Hodgkin disease [36], miRNA expression could vary greatly between these two tumors.

What role might these EBV miRNAs play in NKTCLs? Cancer is a disease where cell proliferation is dysregulated. A number of studies have demonstrated a connection between miRNAs and cellular differentiation and in many instances miRNAs act as oncogenes by down-regulating tumor suppressors [30,37]. In this study, we found that inhibiting EBV miRNAs slowed the growth rate of NKTCLs. This reduction in proliferation was not because of loss of cell viability. These EBV miRNAs may be functionally analogous to cellular miRNAs like miR- 106b that targets the cell cycle inhibitor $p21^{Cip1}$ [38] or miR-221 and miR-222 that regulate $p27^{kip1}$ [39]. Since EBV miRNAs are evolutionarily conserved [3], it is also possible that they target viral proteins as is the case with EBV-miR-BART17-5p that has been reported to regulate LMP1 [11] or EBV-miR-BART2 that down-regulates BALF5 viral DNA polymerase [10]. In the SNK6 cell line we observed that inhibiting EBV-miR-BART9 reduced the level of LMP1 mRNA and protein. Furthermore, over-expression of BART9 miRNA resulted in increase of LMP1 protein and transcript levels. This suggests that in NKTCLs, BART9 miRNA likely regulates LMP1 mRNA expression and we favor the hypothesis that this is an indirect regulation as a reporter plasmid containing the 3′ UTR of the LMP1 mRNA was not responsive to BART9 in transient expression experiments (data not shown). BART9 may indirectly up-regulate LMP1 by targeting a repressor of its expression. When BART9 is inhibited, the level of this putative repressor may be increased resulting in decrease of LMP1 transcript and protein levels. Alternatively, BART9 may be involved somehow in maintaining LMP1 mRNA stability which has been reported to have a long half-life [40]. In this scenario, BART9 may stabilize LMP1 mRNA, and inhibition of BART9 thus renders the LMP1 mRNA susceptible to degradation.

A tight regulation on the expression of LMP1 is beneficial to EBV and its survival in infected cells. For instance, if LMP1 expression is consistently high, it can either result in cell growth arrest [41], inhibit viral and cellular promoters [42] or enhance epitope presentation to cytotoxic T cells [43]. However, under certain conditions, it might be beneficial for EBV to induce LMP1 expression for a short period of time. Notably, a recent study reported the transient upregulation of LMP1 by the p38 signaling pathway [44].

In summary, we have shown that 19 EBV miRNAs are abundantly expressed in NKTCLs and their levels are likely to be important in maintaining cell growth. Our data also indicate that EBV BART9 is involved in regulating LMP-1 expression in these cells. This has implications in mechanisms of lymphomagenesis and future experiments could be directed at investigating the role of EBV miRNAs and its regulation of cellular targets.

Methods

Cell lines

The NK-T cell lymphoma (NKTCL) cell lines, SNK6, SNK10, SNT8, SNT15, SNT16 were obtained from Norio Shimizu (Tokyo Medical and Dental University). The cells were cultured in RPMI1640 supplemented with 10% fetal bovine serum, 1%

A

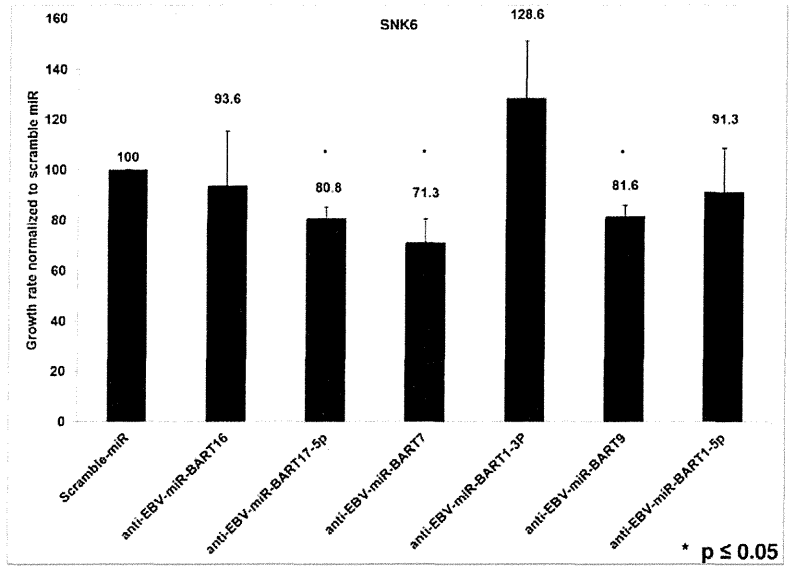
SNK6
Growth rate normalized to scramble miR
160
140
120
100
80
60
40
20
0
100
93.6
80.8
71.3
128.6
81.6
91.3
Scramble-miR
anti-EBV-miR-BART16
anti-EBV-miR-BART17-5p
anti-EBV-miR-BART7
anti-EBV-miR-BART1-3P
anti-EBV-miR-BART9
anti-EBV-miR-BART1-5p
* p ≤ 0.05

B

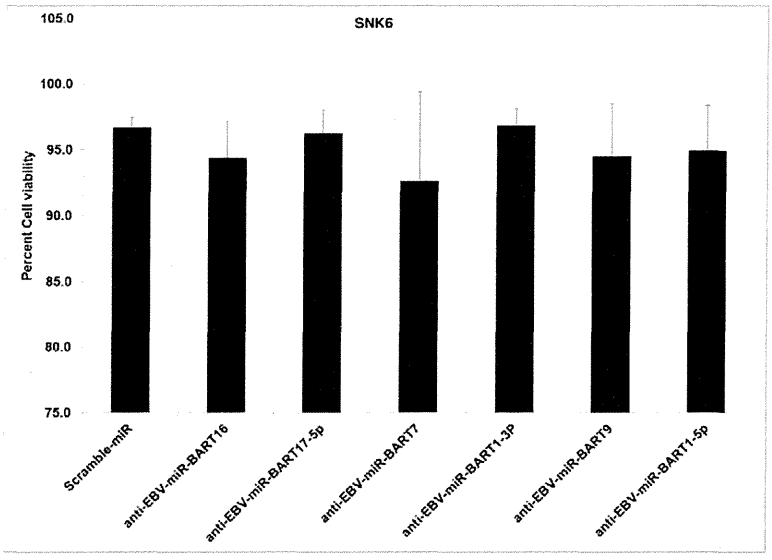
SNK6
Percent Cell viability
105.0
100.0
95.0
90.0
85.0
80.0
75.0
Scramble-miR
anti-EBV-miR-BART16
anti-EBV-miR-BART17-5p
anti-EBV-miR-BART7
anti-EBV-miR-BART1-3P
anti-EBV-miR-BART9
anti-EBV-miR-BART1-5p

C

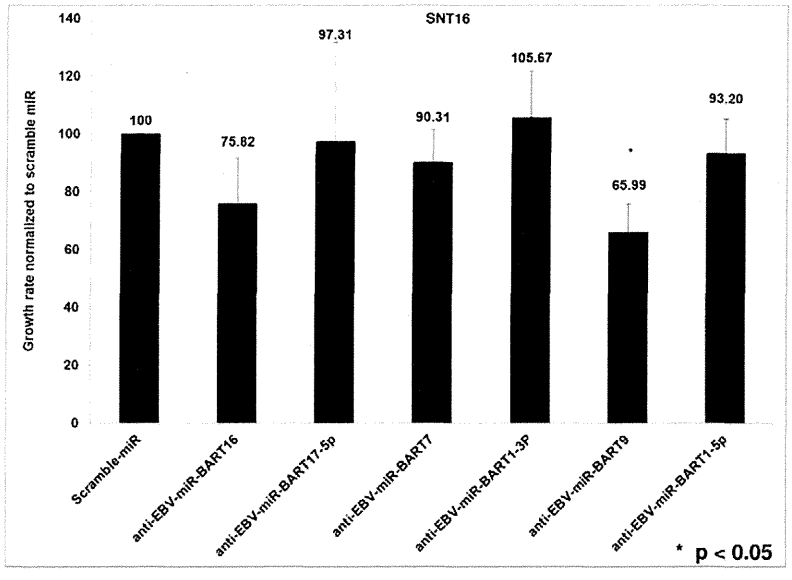
SNT16
Growth rate normalized to scramble miR
140
120
100
80
60
40
20
0
100
75.82
97.31
90.31
105.67
65.99
93.20
Scramble-miR
anti-EBV-miR-BART16
anti-EBV-miR-BART17-5p
anti-EBV-miR-BART7
anti-EBV-miR-BART1-3P
anti-EBV-miR-BART9
anti-EBV-miR-BART1-5p
* p < 0.05

Figure 3. Inhibiting EBV BART miRNA levels affect NKTCL growth rate without affecting cell viability. (**A**) SNK6 cells were transfected with antisense to the indicated EBV miRNAs and cell numbers counted every 24 hours for three days. Cell growth rate was calculated as difference in cell numbers between the 24 hour and 72 hour time point and compared with cells transfected with control Scramble miRNA. Data shown are the average ± SD from three independent experiments. (* represents p value of ≤0.05 in a paired t-test). (**B**) SNK6 transfected with antisense EBV miRNAs were analyzed for viability by Trypan blue exclusion in a Vi-CELL counter every 24 hours for three days. The data presented is the cell viability at 72 hours post-transfection and is the average ± SD from three independent experiments. (**C**) SNT16 cells were transfected with antisense to the indicated EBV miRNAs and cell growth rate analyzed as described above. Data shown are the average ± SD from three independent experiments. (* represents p value of <0.05 in a paired t-test).
doi:10.1371/journal.pone.0027271.g003

Penicillin-Streptomycin and 250 ng/ml Fungizone (Amphotericin B; Invitrogen) and 600 IU of IL-2.

MiRNA microarray analysis and validation

Total RNA was isolated from SNK6 and SNT16 cells using the miRNAeasy kit (Qiagen) as per manufacturer's protocol. RNA was analyzed by LC Sciences (Houston, TX) with miRNA microarrays using the μParaflo microfluidic chip technology and all data is MIAME compliant. The detailed process can be found at http://www.lcsciences.com. Briefly, photogenerated reagent chemistry probes for miRNAs were *in situ* synthesized on chips with three repeats for each probe to allow for statistical analysis. MiRHumanViruses version 13 arrays were used to detect a total of 1100 unique mature miRNAs comprising of 875 human miRNAs and 225 virus miRNAs. The virus miRNAs included 44 EBV miRNAs. RNA samples from SNK6 and SNT16 cells were labeled with Cy3 for hybridization. The chips included 50 control probes based on Sanger miRBase Release 13 with four-sixteen repeats. The control probes were used for quality controls of chip production, sample labeling and assay conditions. Included in the control probes were PUC2PM-20B and PUC2MM-20B which are the perfect match and single-base match detection probes, respectively, of a 20-mer RNA positive control sequence that is spiked into the RNA samples before labeling. For a transcript to be listed as detectable three conditions had to be met: (1) signal intensity had to be greater than three times background standard deviation; (2) spot co-variance (CV), defined as ratio of standard deviation over signal intensity had to be less than 0.5; (3) the signals from at least 50% of the repeating probes had to be above detection level. Data was normalized using a cyclic LOWESS (Locally-weighted Regression) method [45] to remove system related variations such as sample amount variations, dye labeling bias, and signal gain differences between scanners to reveal biological relevant variations. A t-test was performed on the signals obtained for the repeating probes and p-value calculated. MiRNAs were defined as differentially expressed if they had a p-value<0.01. Clustering analysis was performed with a hierarchical method using average linkage and Euclidean distance metric. The clustering data was represented as a heat map using TIGR MeV (Multiple Experimental Viewer; The Institute for Genomic Research). The microarray data has been deposited in GEO database with accession number GSE30695.

Validation of miRNA microarray

Selected EBV miRNAs were quantified using a PCR protocol described by Chen *et al* [46] for detecting miRNAs. Briefly, stem-loop primers complementary to specific EBV miRNAs were designed as described by Cosmopoulos *et al* [19]. For each miRNA assayed, 100 ng of total RNA was reverse transcribed using a TaqMan MicroRNA RT kit as described by the manufacturer and a specific stem-loop primer at a final concentration of 50 nM. RNA was prepared using an RNeasy kit (Qiagen) from exponentially growing tissues culture cells. Each 20 ul PCR reaction contained 1 ul of RT product, 1×TaqMan Universal master mix, 1.5 uM forward primer, 0.7 uM reverse primer, and 0.2 uM probe. The reactions were incubated in a 48-well plate at 95°C for 3 min, followed by 40 cycles of 95°C for 15 s and 60°C for 30 s. The copy number of each of the miRNAs was determined by reverse transcription and amplification of synthetic miRNAs that were identical to the published sequences.

miRNAs and transfection

The miRCURY locked nucleic acid (LNA) modified antisense oligonucleotides to EBV BART miRNAs (anti-EBV-miR-BART) were purchased from Exiqon. The sequence of the antisense oligonucleotides are as follows: Scramble Negative Control (5′-GTGTAACACGTCTATACGCCCA -3′); anti-EBV-miR-BART9 (5′- ACTACGGGACCCATGAAGTGTTA- 3′); anti-EBV-miR-BART17-5p (5′- CTTGTATGCCTGCGTCCTCTTA-3′); anti-EBV-miR-BART7 (5′- CCCTGGACACTGGACTATGATG-3′); anti-EBV-miR-BART1-3p (5′- GACATAGTGGATAGCGGTG-CTA-3′); anti-EBV-miR-BART1-5p (5′- CACAGCACGTCAC-TTCCACTAAGA-3′); anti-EBV-miR-BART16 (5′FAM- AGAG-CACACACCCACTCTATCTAA-3′). Precursor EBV miRNA (pre-EBV-miR) was designed based on the sequence in miRBase sequence database (http://microrna.sanger.ac.uk/sequences). pre-EBV-miR-BART9 (5′- UAACACUUCAUGGGUCCCGUAGU-3′) and precursor Negative control miRNA (pre-NegCtrl) were ordered from Ambion/Applied Biosystems.

SNK6 and SNT 16 cells were seeded at 1×10^6 cells in 24- well tissue culture plates and transfected with antisense or precursor miRNAs using Oligofectamine or Lipofectamine RNAimax according to the manufacturer's protocol. Transfection efficiency of the miRNAs in SNK6 and SNT 16 cells was determined with FAM labeled EBV- BART16 miRNA and was found to be nearly 98% as determined by flow cytometry (data not shown). Cell viability following transfections was measured by Trypan Blue exclusion and found to be ~95%.

RT-real time PCR for EBV mRNAs

Independent transfections of anti-EBV-miR-BART 9 or pre-EBV-miR-BART 9 were performed in SNK6 cells. The controls transfected were either Scramble-miRNA (Exiqon) or Precursor-Negative Control (Pre-NegCtrl) (Applied Biosystems), respectively, as described above. Total RNA was isolated using RNeasy mini kit (Qiagen) and RT-real-time-PCR assays carried out for quantification of LMP1 and α-tubulin levels using the Bio-Rad MyIQ single color detection system. Briefly, 10 ng of cellular RNA was reverse transcribed into cDNA using the iScript cDNA synthesis kit (Bio-Rad) in a 20 μl reaction using the manufacturer's protocol. Quantitative real-time PCR was performed using 3 μl of the synthesized cDNA and the iQ™ SYBR Green Supermix (Bio-Rad). PCR reactions were carried out in 96-well format using a Bio-Rad iCycler. Analysis was done by the MyIQ software program (Bio-Rad) and the fold-changes were calculated using the ΔΔCt method as previously described [47] with α-Tubulin as the housekeeping gene control. The primer sequences used for LMP1 have been described previously [48] and were LMP1 (forward) - 5′

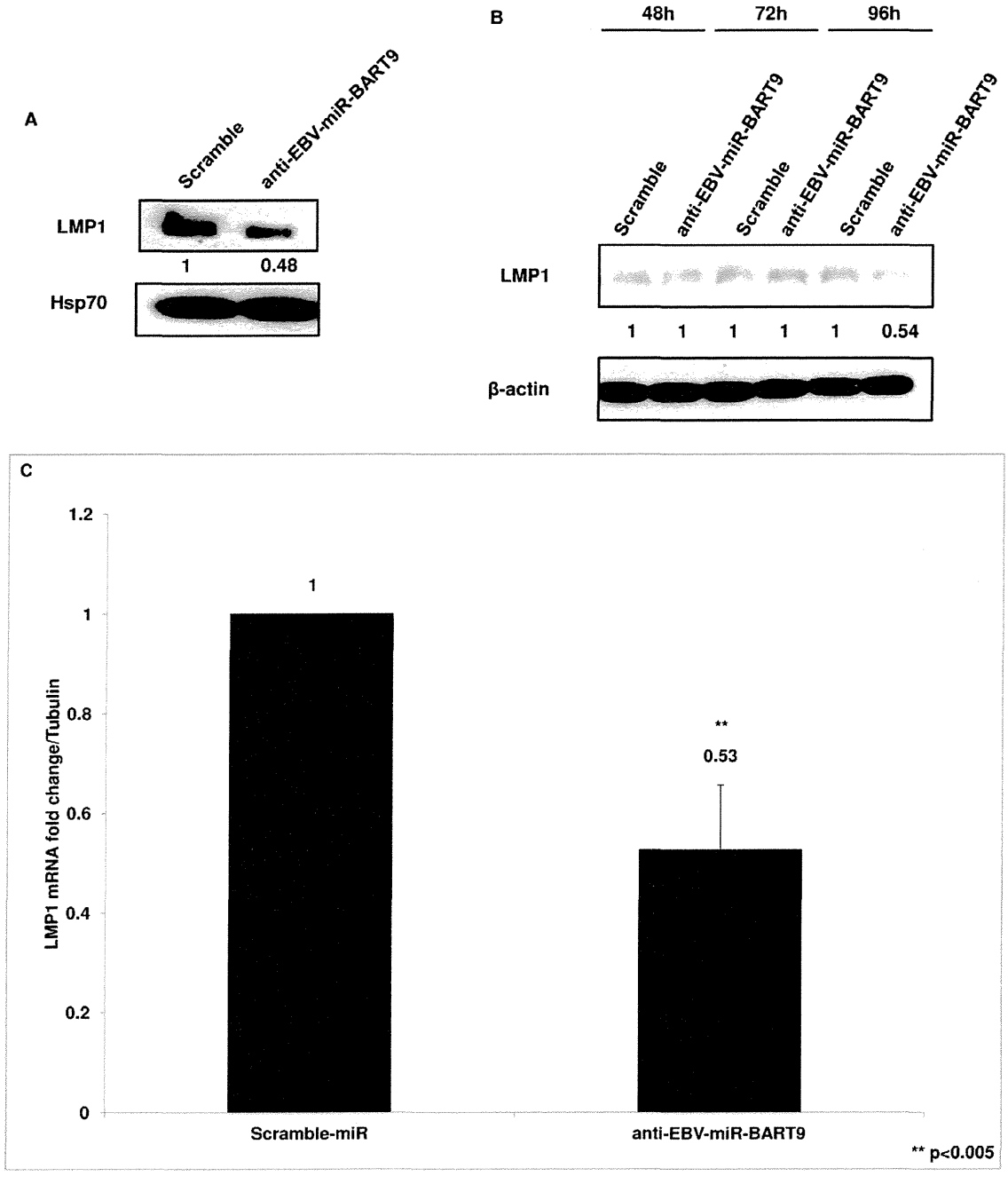

Figure 4. Immunoblot and Q-RT-PCR analysis of LMP1 expression in SNK6 following inhibition of EBV-BART9 miRNA. (**A**) SNK6 cells were transfected with anti-EBV-BART9 miRNA or Scramble control miRNA and cell lysates prepared 96 hours post-transfection. LMP1 protein expression was analyzed in immunoblots. When compared to cells transfected with control miRNA and normalized to β-actin loading control, quantification of immunoblots showed that BART9 inhibition reduced LMP1 protein levels by ~50%. (**B**) SNK6 cells were transfected with control or anti-EBV-BART9 miRNA and samples collected every 24 hours in a time-course experiment. Cell lysates were prepared and immunoblot analysis carried out to determine LMP1 expression. Quantification of LMP1 levels using Image J as described above showed that LMP1 protein levels are reduced only at later time-point. (**C**) SNK6 cells were transfected with either anti-EBV-BART9 or control miRNA and cells collected 96 hours post-transfection. Total RNA was extracted and cDNA synthesized using iScript cDNA synthesis kit. Using LMP1 specific primers, Q-PCR was carried out and data analyzed using the ΔΔCt method. Data shown is the average ± SD from three independent experiments. (** represents p value of <0.005 in a paired t-test).
doi:10.1371/journal.pone.0027271.g004

AGCCCTCCTTGTCCTCTATTCCTT 3′, LMP1 (reverse) - 5′ACCAAGTCGCCAGAGAATCTCCAA 3′. The primers for α-Tubulin were, α-Tubulin (forward) - 5′ CCTGACCACCCACACCACAC 3′, α-Tubulin (reverse) - 5′ TCTGACTGATGAGGCGGTTGAG 3′.

Cell proliferation functional assay

SNK6 and SNT16 cells were seeded in 96 well plates at 8×10^5 cells in 100 μl/well and transfected with 100 pmol of indicated anti-EBV-miRNAs or pre-EBV-miRNAs or control Scramble-miRNA or Pre-Neg-Ctrl. In some experiments, the cells were

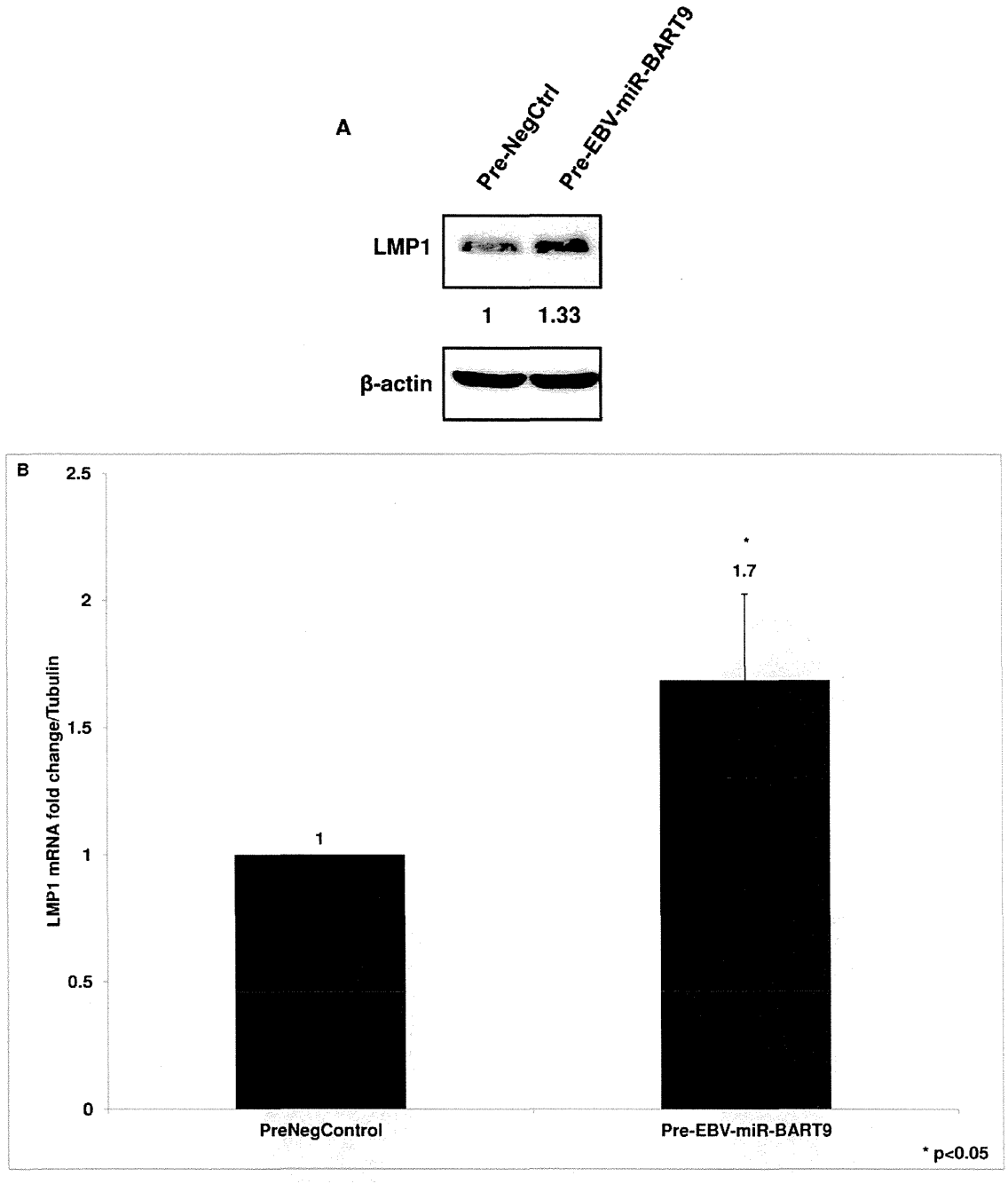

Figure 5. Precursor EBV-BART9 miRNA increases LMP1 protein and mRNA levels in SNK6 cells. (**A**) SNK6 cells were transfected with precursor EBV-BART9 or control miRNA. The cells were collected 96 hours post-transfection and cell lysates prepared for immunoblot analysis. Quantification of immunoblots showed a ~33% increase in LMP1 protein levels in cells transfected with EBV miRNA compared to control miRNA transfected cells when normalized to loading control. Data shown is a representative immunoblot from three independent experiments. (**B**) Total RNA was extracted from SNK6 cells transfected with precursor EBV-BART9 or control miRNA. Following cDNA synthesis, LMP1 mRNA levels were analyzed by Q-RT-PCR. Data presented is the average ± SD from three independent experiments. (* represents p value of <0.05 in a paired t-test).
doi:10.1371/journal.pone.0027271.g005

seeded at 1×10^6 cells/well. After overnight incubation, the cells were transferred into 24 well tissue culture plates. Cells were collected every 24 hours and analyzed for cell number and viability using the Becton-Dickinson Vi-CELL counter at the Baylor College of Medicine Flow Cytometry Core. The cell counter uses trypan blue exclusion to automatically stain and count cells, as well as assay cell size and viability.

Immunoblotting

Cells following treatment were lysed with EBCD buffer (50 mM Tris-HCl, pH 8.0, 120 mM NaCl, 0.5% NP-40, 5 mM dithiothreitol) containing protease inhibitor cocktail (Sigma). Immunoblotting was performed as described previously [49]. Monoclonal antibodies used in this study include, LMP1 (S12), EBNA-LP (JF186), EBNA3C (A10), and EBNA2 (R3). Other antibodies

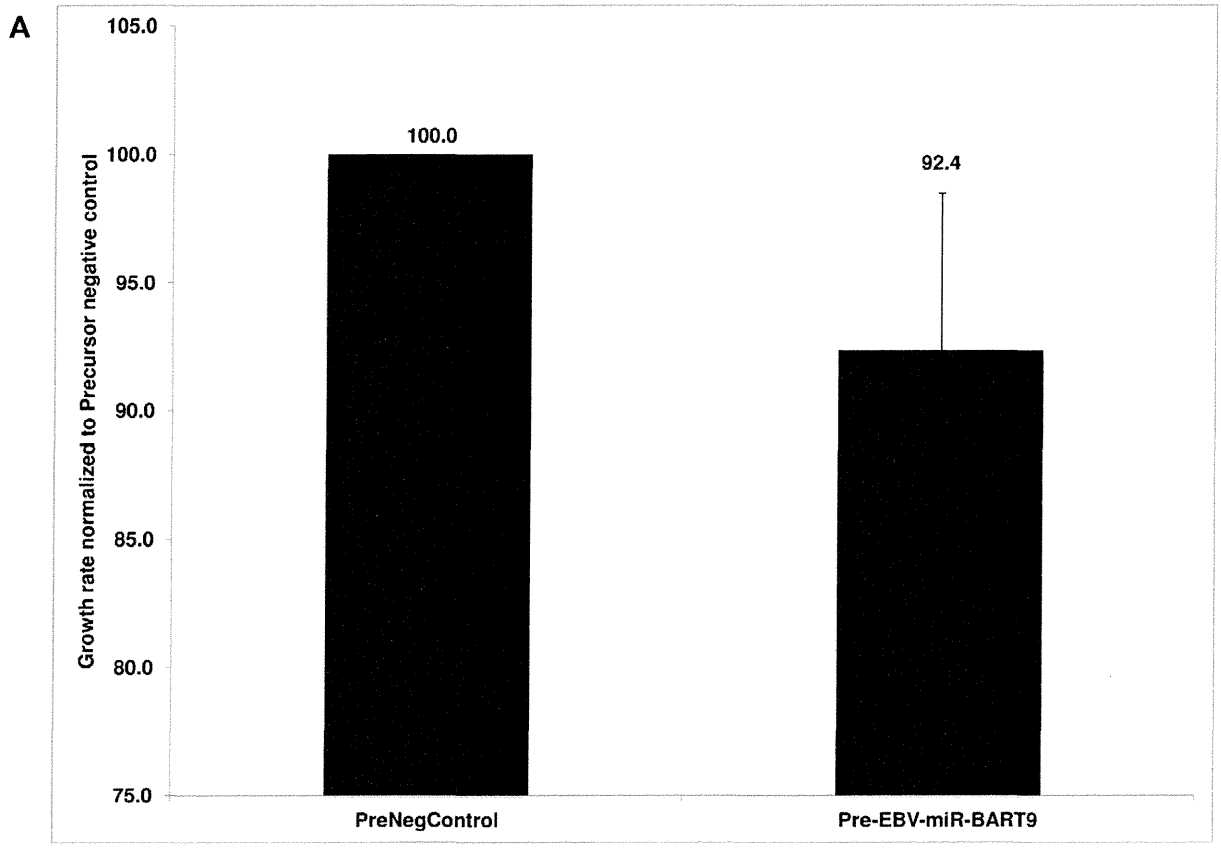
A
105.0
100.0
95.0
90.0
85.0
80.0
75.0
Growth rate normalized to Precursor negative control
100.0
92.4
PreNegControl
Pre-EBV-miR-BART9

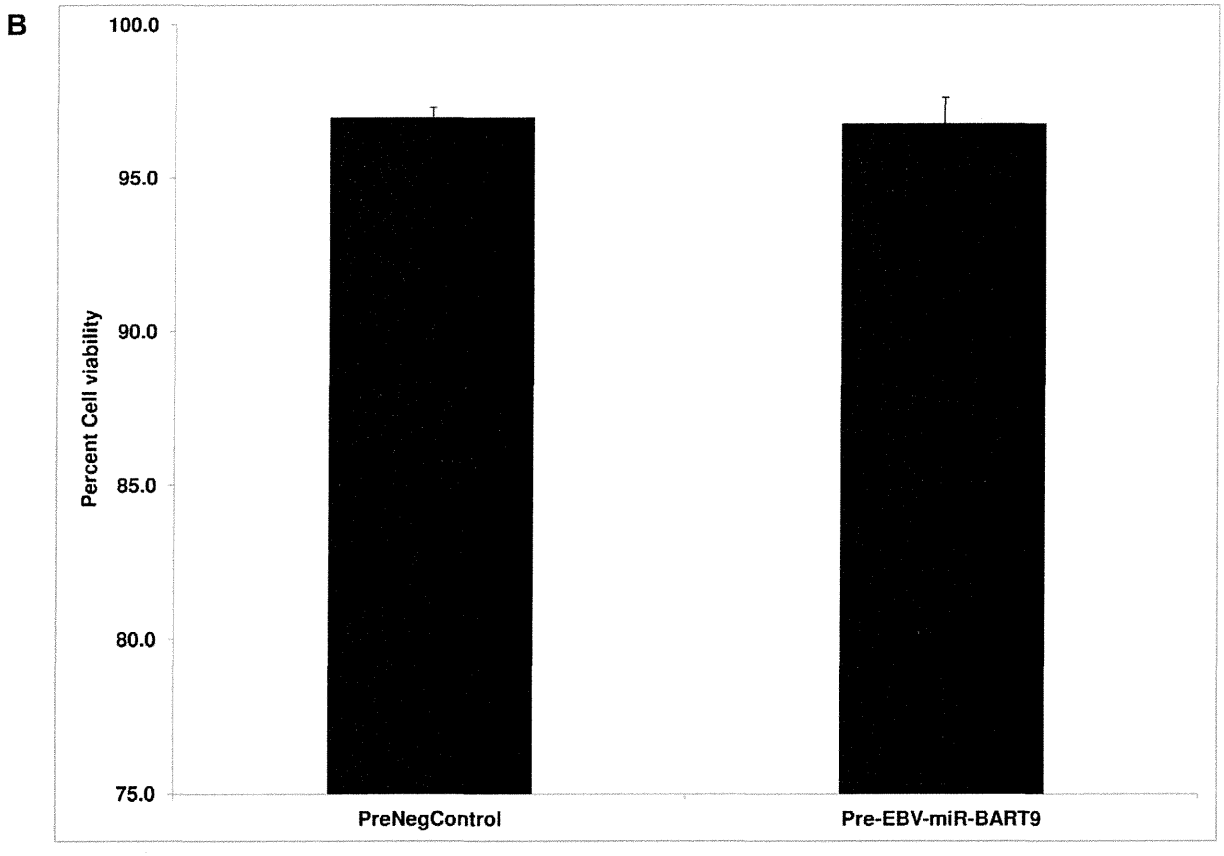
B
100.0
95.0
90.0
85.0
80.0
75.0
Percent Cell viability
PreNegControl
Pre-EBV-miR-BART9

Figure 6. Increasing EBV-BART9 miRNA level has a subtle effect on SNK6 growth rate. (**A**) Precursor EBV-BART9 miRNA or control miRNA were transfected into SNK6 cells and samples collected every 24 hours for three days. Growth rate of SNK6 cells was determined by calculating cell numbers. When normalized to cell numbers in control miRNA transfected cells, there was ~8% reduction in SNK6 growth rate. The data shown is the average ± SD from three independent experiments. (**B**) In the experiments described above, SNK6 were analyzed for viability by Trypan blue exclusion in a Vi-CELL counter at every time point. The data shown is the cell viability at 72 hours post-transfection and is the average ± SD from three independent experiments.
doi:10.1371/journal.pone.0027271.g006

obtained commercially included EBNA1 (1EB12, Santa Cruz), Zta (Argene), β-Actin (Sigma) and α-tubulin (Sigma). HRP secondary antibodies were obtained from Jackson Immunolaboratories and Western blots were developed using the SuperSignal West pico kit (Thermo Scientific). Immunoblots were quantified using Image J software [50].

Acknowledgments

We acknowledge Baylor College of Medicine Cytometry Core for flow cytometry analysis.

Author Contributions

Conceived and designed the experiments: RR APR PDL. Performed the experiments: RR HD DG JT PDL. Analyzed the data: RR HD DG JT PDL. Contributed reagents/materials/analysis tools: NS. Wrote the paper: RR APR PDL.

References

1. Shah KM, Young LS (2009) Epstein-Barr virus and carcinogenesis: beyond Burkitt's lymphoma. Clin Microbiol Infect 15: 982–988.
2. Thorley-Lawson DA (2005) EBV the prototypical human tumor virus–just how bad is it? J Allergy Clin Immunol 116: 251–261; quiz 262.
3. Cai X, Schafer A, Lu S, Bilello JP, Desrosiers RC, et al. (2006) Epstein-Barr virus microRNAs are evolutionarily conserved and differentially expressed. PLoS Pathog 2: e23.
4. Chen SJ, Chen GH, Chen YH, Liu CY, Chang KP, et al. (2010) Characterization of Epstein-Barr virus miRNAome in nasopharyngeal carcinoma by deep sequencing. PLoS One 5.
5. Grundhoff A, Sullivan CS, Ganem D (2006) A combined computational and microarray-based approach identifies novel microRNAs encoded by human gamma-herpesviruses. RNA 12: 733–750.
6. Pfeffer S, Sewer A, Lagos-Quintana M, Sheridan R, Sander C, et al. (2005) Identification of microRNAs of the herpesvirus family. Nat Methods 2: 269–276.
7. Pratt ZL, Kuzembayeva M, Sengupta S, Sugden B (2009) The microRNAs of Epstein-Barr Virus are expressed at dramatically differing levels among cell lines. Virology 386: 387–397.
8. Selbach M, Schwanhausser B, Thierfelder N, Fang Z, Khanin R, et al. (2008) Widespread changes in protein synthesis induced by microRNAs. Nature 455: 58–63.
9. Cullen BR (2009) Viral and cellular messenger RNA targets of viral microRNAs. Nature 457: 421–425.
10. Barth S, Pfuhl T, Mamiani A, Ehses C, Roemer K, et al. (2008) Epstein-Barr virus-encoded microRNA miR-BART2 down-regulates the viral DNA polymerase BALF5. Nucleic Acids Res 36: 666–675.
11. Lo AK, To KF, Lo KW, Lung RW, Hui JW, et al. (2007) Modulation of LMP1 protein expression by EBV-encoded microRNAs. Proc Natl Acad Sci U S A 104: 16164–16169.
12. Choy EY, Siu KL, Kok KH, Lung RW, Tsang CM, et al. (2008) An Epstein-Barr virus-encoded microRNA targets PUMA to promote host cell survival. J Exp Med 205: 2551–2560.
13. Xia T, O'Hara A, Araujo I, Barreto J, Carvalho E, et al. (2008) EBV microRNAs in primary lymphomas and targeting of CXCL-11 by ebv-mir-BHRF1-3. Cancer Res 68: 1436–1442.
14. Cameron JE, Fewell C, Yin Q, McBride J, Wang X, et al. (2008) Epstein-Barr virus growth/latency III program alters cellular microRNA expression. Virology 382: 257–266.
15. Cameron JE, Yin Q, Fewell C, Lacey M, McBride J, et al. (2008) Epstein-Barr virus latent membrane protein 1 induces cellular MicroRNA miR-146a, a modulator of lymphocyte signaling pathways. J Virol 82: 1946–1958.
16. Lu F, Weidmer A, Liu CG, Volinia S, Croce CM, et al. (2008) Epstein-Barr virus-induced miR-155 attenuates NF-kappaB signaling and stabilizes latent virus persistence. J Virol 82: 10436–10443.
17. Yin Q, McBride J, Fewell C, Lacey M, Wang X, et al. (2008) MicroRNA-155 is an Epstein-Barr virus-induced gene that modulates Epstein-Barr virus-regulated gene expression pathways. J Virol 82: 5295–5306.
18. Amoroso R, Fitzsimmons L, Thomas WA, Kelly GL, Rowe M, et al. (2011) Quantitative studies of Epstein-Barr virus-encoded microRNAs provide novel insights into their regulation. J Virol 85: 996–1010.
19. Cosmopoulos K, Pegtel M, Hawkins J, Moffett H, Novina C, et al. (2009) Comprehensive profiling of Epstein-Barr virus microRNAs in nasopharyngeal carcinoma. J Virol 83: 2357–2367.
20. Imig J, Motsch N, Zhu JY, Barth S, Okoniewski M, et al. (2011) microRNA profiling in Epstein-Barr virus-associated B-cell lymphoma. Nucleic Acids Res 39: 1880–1893.
21. Kim do N, Chae HS, Oh ST, Kang JH, Park CH, et al. (2007) Expression of viral microRNAs in Epstein-Barr virus-associated gastric carcinoma. J Virol 81: 1033–1036.
22. Nagata H, Konno A, Kimura N, Zhang Y, Kimura M, et al. (2001) Characterization of novel natural killer (NK)-cell and gammadelta T-cell lines established from primary lesions of nasal T/NK-cell lymphomas associated with the Epstein-Barr virus. Blood 97: 708–713.
23. Zhang Y, Nagata H, Ikeuchi T, Mukai H, Oyoshi MK, et al. (2003) Common cytological and cytogenetic features of Epstein-Barr virus (EBV)-positive natural killer (NK) cells and cell lines derived from patients with nasal T/NK-cell lymphomas, chronic active EBV infection and hydroa vacciniforme-like eruptions. Br J Haematol 121: 805–814.
24. Aozasa K, Takakuwa T, Hongyo T, Yang WI (2008) Nasal NK/T-cell lymphoma: epidemiology and pathogenesis. Int J Hematol 87: 110–117.
25. Kohrt H, Advani R (2009) Extranodal natural killer/T-cell lymphoma: current concepts in biology and treatment. Leuk Lymphoma 50: 1773–1784.
26. Tao Q, Young LS, Woodman CB, Murray PG (2006) Epstein-Barr virus (EBV) and its associated human cancers–genetics, epigenetics, pathobiology and novel therapeutics. Front Biosci 11: 2672–2713.
27. Harabuchi Y, Yamanaka N, Kataura A, Imai S, Kinoshita T, et al. (1990) Epstein-Barr virus in nasal T-cell lymphomas in patients with lethal midline granuloma. Lancet 335: 128–130.
28. Ho FC, Srivastava G, Loke SL, Fu KH, Leung BP, et al. (1990) Presence of Epstein-Barr virus DNA in nasal lymphomas of B and 'T' cell type. Hematol Oncol 8: 271–281.
29. Kanavaros P, Lescs MC, Briere J, Divine M, Galateau F, et al. (1993) Nasal T-cell lymphoma: a clinicopathologic entity associated with peculiar phenotype and with Epstein-Barr virus. Blood 81: 2688–2695.
30. Garzon R, Croce CM (2008) MicroRNAs in normal and malignant hematopoiesis. Curr Opin Hematol 15: 352–358.
31. Bueno MJ, Perez de Castro I, Malumbres M (2008) Control of cell proliferation pathways by microRNAs. Cell Cycle 7: 3143–3148.
32. Young LS, Rickinson AB (2004) Epstein-Barr virus: 40 years on. Nat Rev Cancer 4: 757–768.
33. Eliopoulos AG, Dawson CW, Mosialos G, Floettmann JE, Rowe M, et al. (1996) CD40-induced growth inhibition in epithelial cells is mimicked by Epstein-Barr Virus-encoded LMP1: involvement of TRAF3 as a common mediator. Oncogene 13: 2243–2254.
34. Yamanaka Y, Tagawa H, Takahashi N, Watanabe A, Guo YM, et al. (2009) Aberrant overexpression of microRNAs activate AKT signaling via down-regulation of tumor suppressors in natural killer-cell lymphoma/leukemia. Blood 114: 3265–3275.
35. Calin GA, Croce CM (2006) MicroRNA signatures in human cancers. Nat Rev Cancer 6: 857–866.
36. Chiang AK, Tao Q, Srivastava G, Ho FC (1996) Nasal NK- and T-cell lymphomas share the same type of Epstein-Barr virus latency as nasopharyngeal carcinoma and Hodgkin's disease. Int J Cancer 68: 285–290.
37. Esquela-Kerscher A, Slack FJ (2006) Oncomirs - microRNAs with a role in cancer. Nat Rev Cancer 6: 259–269.
38. Ivanovska I, Ball AS, Diaz RL, Magnus JF, Kibukawa M, et al. (2008) MicroRNAs in the miR-106b family regulate p21/CDKN1A and promote cell cycle progression. Mol Cell Biol 28: 2167–2174.
39. Galardi S, Mercatelli N, Giorda E, Massalini S, Frajese GV, et al. (2007) miR-221 and miR-222 expression affects the proliferation potential of human prostate carcinoma cell lines by targeting p27Kip1. J Biol Chem 282: 23716–23724.
40. Sample J, Kieff E (1990) Transcription of the Epstein-Barr virus genome during latency in growth-transformed lymphocytes. J Virol 64: 1667–1674.

41. Kaykas A, Sugden B (2000) The amino-terminus and membrane-spanning domains of LMP-1 inhibit cell proliferation. Oncogene 19: 1400–1410.
42. Narbonnet S, Mariame B (2006) The Epstein-Barr virus oncoprotein LMP1 inhibits the activity of viral or cellular promoters without inducing cytostasis. Virology 350: 381–393.
43. Brooks JM, Lee SP, Leese AM, Thomas WA, Rowe M, et al. (2009) Cyclical expression of EBV latent membrane protein 1 in EBV-transformed B cells underpins heterogeneity of epitope presentation and CD8+ T cell recognition. J Immunol 182: 1919–1928.
44. Johansson P, Jansson A, Ruetschi U, Rymo L (2010) The p38 signaling pathway upregulates expression of the Epstein-Barr virus LMP1 oncogene. J Virol 84: 2787–2797.
45. Bolstad BM, Irizarry RA, Astrand M, Speed TP (2003) A comparison of normalization methods for high density oligonucleotide array data based on variance and bias. Bioinformatics 19: 185–193.
46. Chen C, Ridzon DA, Broomer AJ, Zhou Z, Lee DH, et al. (2005) Real-time quantification of microRNAs by stem-loop RT-PCR. Nucleic Acids Res 33: e179.
47. Haaland RE, Yu W, Rice AP (2005) Identification of LKLF-regulated genes in quiescent CD4+ T lymphocytes. Mol Immunol 42: 627–641.
48. Goormachtigh G, Ouk TS, Mougel A, Tranchand-Bunel D, Masy E, et al. (2006) Autoactivation of the Epstein-Barr virus oncogenic protein LMP1 during type II latency through opposite roles of the NF-kappaB and JNK signaling pathways. J Virol 80: 7382–7393.
49. Ramakrishnan R, Dow EC, Rice AP (2009) Characterization of Cdk9 T-loop phosphorylation in resting and activated CD4(+) T lymphocytes. J Leukoc Biol 86: 1345–1350.
50. Abramoff MD, Magelhaes PJ, Ram SJ (2004) Image Processing with ImageJ. Biophotonics International 11: 36–42.

Biochemical and Biophysical Research Communications 419 (2012) 188–193

Contents lists available at SciVerse ScienceDirect

Biochemical and Biophysical Research Communications

journal homepage: www.elsevier.com/locate/ybbrc

Bioluminescent system for dynamic imaging of cell and animal behavior

Chikako Hara-Miyauchi [a,b,c], Osahiko Tsuji [a,d], Aki Hanyu [e], Seiji Okada [f], Akimasa Yasuda [a,d], Takashi Fukano [b], Chihiro Akazawa [c], Masaya Nakamura [d], Takeshi Imamura [g,h], Yumi Matsuzaki [a], Hirotaka James Okano [a,i,*], Atsushi Miyawaki [b,j,*], Hideyuki Okano [a,k,*]

[a] Department of Physiology, Keio University School of Medicine, Tokyo 160-8582, Japan
[b] Laboratory for Cell Function Dynamics, Brain Science Institute, RIKEN, Saitama 351-0198, Japan
[c] Department of Biophysics and Biochemistry, Graduate School of Health Care Sciences, Tokyo Medical and Dental University, Tokyo 113-8510, Japan
[d] Department of Orthopedic Surgery, Keio University School of Medicine, Tokyo 160-8582, Japan
[e] Division of Biochemistry, The Cancer Institute of the Japanese Foundation for Cancer Research, Tokyo 135-8550, Japan
[f] Department of Advanced Medical Initiatives, Faculty of Medical Sciences, Kyushu University, Fukuoka 812-8582, Japan
[g] Department of Molecular Medicine for Pathogenesis, Ehime University Graduate School of Medicine, Toon, Ehime 791-0295, Japan
[h] Core Research for Evolutional Science and Technology, The Japan Science and Technology Corporation, Tokyo 135-8550, Japan
[i] Division of Regenerative Medicine Jikei University School of Medicine, Tokyo 150-8461, Japan
[j] Life Function and Dynamics, ERATO, JST, 2-1 Hirosawa, Wako-city, Saitama 351-0198, Japan
[k] RIKEN Keio University Joint Research Laboratory, Brain Science Institute, RIKEN, Saitama 351-0198, Japan

ARTICLE INFO

Article history:
Received 21 January 2012
Available online 5 February 2012

Keywords:
Bioluminescence
Chemiluminescence
Fluorescent protein
Luciferase
Transgenic mouse

ABSTRACT

The current utility of bioluminescence imaging is constrained by a low photon yield that limits temporal sensitivity. Here, we describe an imaging method that uses a chemiluminescent/fluorescent protein, *ff*Luc-cp156, which consists of a yellow variant of *Aequorea* GFP and firefly luciferase. We report an improvement in photon yield by over three orders of magnitude over current bioluminescent systems. We imaged cellular movement at high resolution including neuronal growth cones and microglial cell protrusions. Transgenic *ff*Luc-cp156 mice enabled video-rate bioluminescence imaging of freely moving animals, which may provide a reliable assay for drug distribution in behaving animals for pre-clinical studies.

1. Introduction

In live imaging, fluorescent proteins such as *Aequorea* GFPs and GFP-like proteins are widely used [1,2]. Recently, however, chemiluminescent proteins have also shown promise as powerful tools for biological imaging [3–5]. The significant advantages of bioluminescence over fluorescence imaging include a low background signal, the ability to observe luminescence without excitation light, and the resultant preservation of delicate subcellular organelles and structures during long term imaging protocols. However, because of their weak luminescence, it is difficult to use chemiluminescent proteins for optical imaging of cultured living cells or in freely moving animals. With chemical and genetic modifications of either proteins or substrates brighter and more diverse colors of bioluminescent probes continue to be developed [6–9], including the recently released NanoLuc (Promega). In addition, radiationless energy transfer can improve bioluminescent probes, i.e., if a chemiluminescent probe has a high emissive rate, its excited-state energy can be used to induce the emission of an appropriately positioned fluorescent protein. For example, coupling a green-emitting variant of *Aequorea* GFP to the calcium-sensitive photoprotein aequorin (derived from *Aequorea victoria*) improves its light emission properties. This protein, GFP-aequorin, has been used to perform *in vivo* bioluminescence imaging of calcium signaling in the brain of *Drosophila* [10]. Also, a yellow-emitting variant of *Aequorea* GFP (EYFP) and the *Renilla* luciferase have been concatenated to promote energy transfer from luciferase-bound oxyluciferin to EYFP's chromophore [11]. However, even these new variants do not approach the temporal resolution needed for adequate live imaging.

The fusion of a fluorescent protein to a chemiluminescent protein may cause other effects, such as changes in stability or enzymatic activity that could in turn improve photon yield. In this study, we explored the effect of these modifications by concatenating firefly luciferase (Luc2, Promega) with a yellow-emitting variant of *Aequorea* GFP. The resulting chimeric protein, *ff*Luc-cp156, showed greatly improved performance in bioluminescence imaging, allowing us to observe cultured cells and transgenic mice with a high spatiotemporal resolution over extended periods of time

* Corresponding authors. Addresses: Department of Physiology, Keio University School of Medicine, Tokyo 160-8582, Japan (H. Okano), Laboratory for Cell Function Dynamics, Brain Science Institute, RIKEN, Saitama 351-0198, Japan (A. Miyawaki), Division of Regenerative Medicine, Jikei University School of Medicine, Tokyo 150-8461, Japan (H. J. Okano).

E-mail addresses: hidokano@a2.keio.jp (H. Okano), matsushi@brain.riken.jp (A. Miyawaki), hjokano@jikei.ac.jp (H.J. Okano).

0006-291X/$ - see front matter © 2012 Elsevier Inc. All rights reserved.
doi:10.1016/j.bbrc.2012.01.141

without any excitation light. Since the spectrum of Luc2's emission does not overlap with the spectrum of Venus's absorption, there was no radiationless energy transfer between them. However, the new probe created by the concatenation of Luc2 and the circularly permuted Venus appears to have enhanced stability or enzymatic activity.

2. Material and methods

2.1. Construction of *ff*Luc

To generate the *ff*Luc construct, we inserted a restriction site (GAATTC, *Eco*RI) between variants of Venus and firefly luciferase (Luc2). The deletion mutant of Venus lacked 11 C-terminal flexible amino acids; the circularly permuted Venus had been interchanged and reconnected by a short spacer between the original termini [12].

2.2. Measurement of bioluminescent spectra

The emission spectrum of each *ff*Luc construct, expressed in HEK293T cells, was measured using a spectroscopic photometer (F4500, Hitachi).

2.3. Relative intensities of the *ff*Luc bioluminescence

Bioluminescent signals of *ff*Luc-expressing HEK293T cells were measured by photon counting in a Kronos instrument (ATTO). The signal intensity was normalized to cell number.

2.4. Bioluminescence imaging of cultured cells expressing *ff*Luc-cp156

Transfection was performed using Lipofectamine 2000 transfection reagent; 4 μg of plasmid DNA was used for cells in a 35 mm glass bottom dish. Transfected HeLa cells, microglial cells, or neurons were observed using an inverted microscope (Olympus IX71) with a 60× objective lens (N.A. 1.45), a 0.5× TV lens, and a back-illuminated cooled CCD camera (Cascade512B, Roper Scientific). The microglial cells and neurons were prepared from primary cultures of rat brain. Prior to imaging, luciferin solution (Promega, Beetle luciferin potassium salt) was added to the culture medium at a final concentration of 1 mM.

2.5. Animal experiments

The experimental procedures and housing conditions for animals were approved by the Institute's Animal Experiments Committee and all the animals were cared for and treated humanely in accordance with the Institutional Guidelines for Experiments using Animals.

2.6. Bioluminescence imaging of mice using a digital camera

A luciferin solution (150 mg/kg) was administered intraperitoneally to a CAG-*ff*Luc-cp156 transgenic mouse (5 months old). Images were taken in a dark room using a common digital camera (E-330, Olympus) with a 4 s exposure time, 3.5 *F* value, 1600 ISO sensitivity, and 29.0 mm focal length.

2.7. Bioluminescence imaging of anesthetized CAG-*ff*Luc-cp156 transgenic mice

CAG-*ff*Luc-cp156 transgenic mice were anesthetized with a mixture of isoflurane and oxygen. The mice received luciferin (150 mg/kg BW) intravenously, intraperitoneally, or orally. Immediately after luciferin administration, time-lapse or consecutive bioluminescence imaging was initiated, using the IVIS Imaging System 100 Series (Xenogen, Alameda, CA).

2.8. Bioluminescence imaging of freely moving CAG-*ff*Luc-cp156 transgenic mice

Images of moving mice were taken using an *in vivo* imaging system (LumazoneFA, Roper Japan) with a Cascade 512B cooled CCD camera (Roper Scientific). Three administration methods were attempted. First, luciferin (150 mg/kg) was administered to a mouse intraperitoneally. Bioluminescent (BL) images were consecutively collected every 33 ms. Second, luciferin was orally administered voluntarily, as follows: a mouse was water-restricted for several hours, then placed in the system along with 1.5% low-melting agarose that contained luciferin (0.75 mg/mL). BL images (500 ms exposure time) and fluorescent (FL) images (100 ms exposure time) were acquired in alteration; paired BL/FL images were acquired every 5 s. Finally, luciferin was administered percutaneously: a mouse with a depilated back was placed in the system, and vaseline containing 50 mg/g of luciferin powder was applied to its back BL images (1 s exposure time) and FL images (100 ms exposure time) were acquired in alternation; paired BL/FL images were acquired every 5 s.

2.9. Visualization of CAG-*ff*Luc-cp156 embryos in the mother mouse

A wild-type female mouse was crossed with a CAG-*ff*Luc-cp156 transgenic male mouse (homozygous). The pregnant mouse was given an intraperitoneal injection of luciferin (150 mg/kg BW); bioluminescence and fluorescence images were captured by a cooled CCD camera (PIXSIS-2048B, Roper Industries) with a lens of 50 mm focal length (EF50 mm, F1.2L USM, Canon). To take the fluorescence images, the mother mouse was illuminated with LEDs at 470 nm (Luxeon K2 LXK2-PB14-Q00, Lumileds), and the fluorescence from the sample was detected via a band-pass filter (ET535/30m, Chroma Technology).

3. Results and discussion

3.1. Concatenation of Luc2 and Venus to yield *ff*Luc

A modified North American firefly *Photinus pyralis* luciferase, codon-optimized for expression in human cells (Luc2, Promega), was fused with Venus variants containing either a deletion or a series of circular permutations [12] to create *ff*Luc-del or *ff*Luc-cps, respectively (Fig. 1A). After transfection into cultured cells, the bioluminescent spectra of the constructs were measured with a spectrophotometer. The new *ff*Luc constructs showed nearly the same emission spectra, peaking at 620 nm as Luc2 (Fig. 1B). However, the bioluminescence intensities were higher in cells expressing *ff*Luc constructs than in cells expressing Luc2. When quantitated using a photon-counting device (Kronos, ATTO), cell samples containing *ff*Luc-cp156 were several times brighter than samples containing Luc2 (Fig. 1C). Normalization to protein expression level revealed that bioluminescent activity per molecule is similar between *ff*Lucs and Luc2 (Supplementary Fig. S1 online), but *ff*Lucs provided reliably brighter signals from both fluorescence and bioluminescence. *ff*Luc-cp156 was used in further studies.

3.2. Visualization of bioluminescence in single cells using *ff*Luc-cp156

*ff*Luc-cp156 was transfected into cultured HeLa cells. After the addition of luciferin (1 mM), we observed bioluminescent signals from single cells using a standard fluorescence microscope system equipped with an oil-immersion objective lens and a

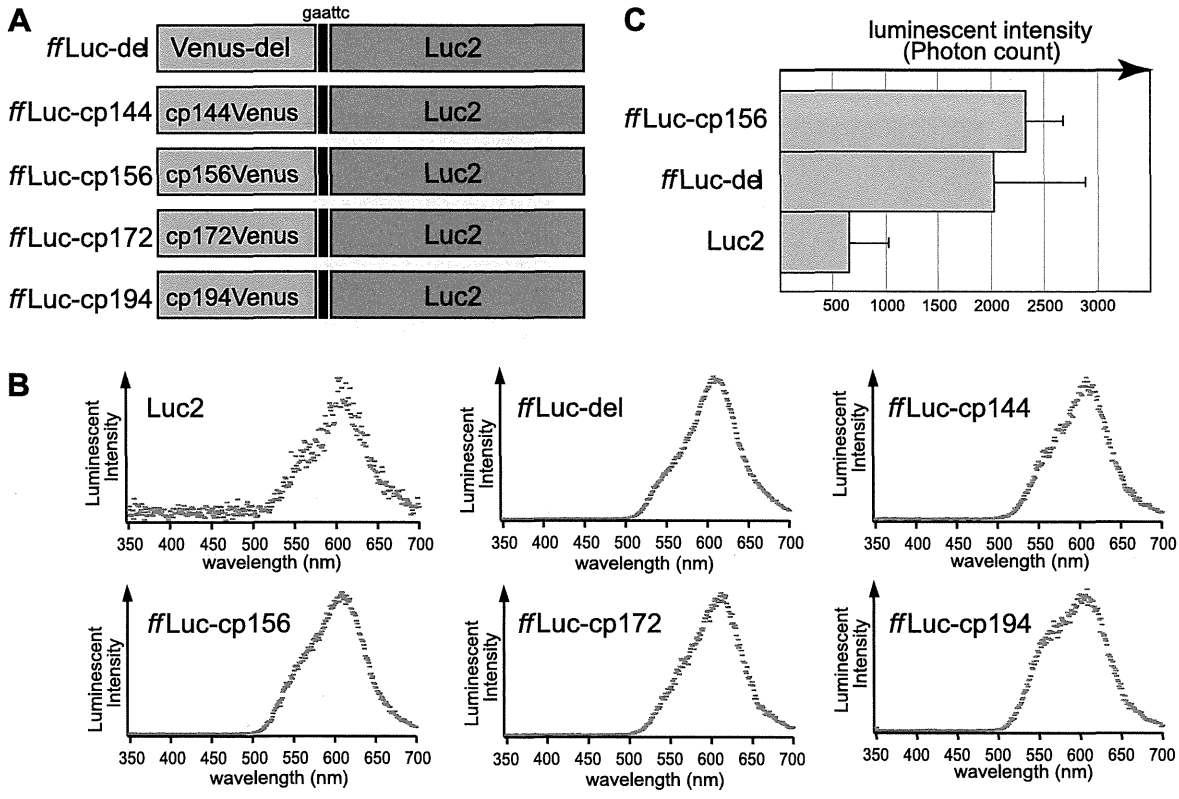

Fig. 1. *ff*Luc constructs. (A) *ff*Luc was constructed as a fusion of a variant of Venus (a deletion mutant or a circularly permuted variant: cp144, cp156, cp172, and cp194) and humanized firefly luciferase (Luc2). GAATTC, the restriction site (*Eco*RI). (B) Bioluminescent spectra of transfected cells. (C) Relative intensities of bioluminescence signals from cells expressing *ff*Luc-cp156, *ff*Luc-del, and Luc2.

back-illuminated EM tip-equipped CCD camera. We first adjusted the focus on cells using phase contrast (PC) images (Fig. 2A), and then selected transfected cells using fluorescence images (Fig. 2B). Next, a 500 ms exposure of the camera yielded a bioluminescence image wherein individual transfected cells were sufficiently resolved (Fig. 2C). When the camera exposure was extended to 5 s, the image quality was greatly improved (Fig. 2D). Furthermore, use of *ff*Luc-cp156 enabled us to capture a series of bioluminescence images of actively migrating microglial cells (Fig. 2E; Supplementary Movie 1 online) and extending growth cones of rat hippocampal neurons (Fig. 2F; Supplementary Movie 2 online) over several consecutive hours. Although the exposure time could be shortened to a few seconds while preserving image quality, we adopted a 30 s exposure as a standard, in order to limit the total amount of data collected over long-term imaging experiments. Bioluminescent signals from cultured cells were sustained for >2 days after the initial addition of luciferin, demonstrating the possibility of long-term *in vivo* observation of cell proliferation and/or differentiation.

3.3. Strong bioluminescence from CAG-*ff*Luc-cp156 transgenic mice

To examine the utility of *ff*Luc-cp156 in living animals, we generated transgenic mice using a construct that consisted of a CAG promoter-driven combination cassette bearing a neomycin-coding sequence sandwiched by two loxP sequences and the *ff*Luc-cp156 gene (Fig. 3A). We cross-bred the line carrying the reporter gene (CAG-neo$^{loxP/loxP}$-*ff*Luc) with a line ubiquitously expressing Cre recombinase (CAG-Cre mice) [13], to yield a mouse line ubiquitously producing *ff*Luc-cp156. When illuminated with blue light, the CAG-*ff*Luc-cp156 mice emitted yellow fluorescence. After dissection, we investigated the fluorescence of various organs and tissues using a fluorescence stereomicroscope. Fluorescence from Venus was observed in almost all tissues examined, with the

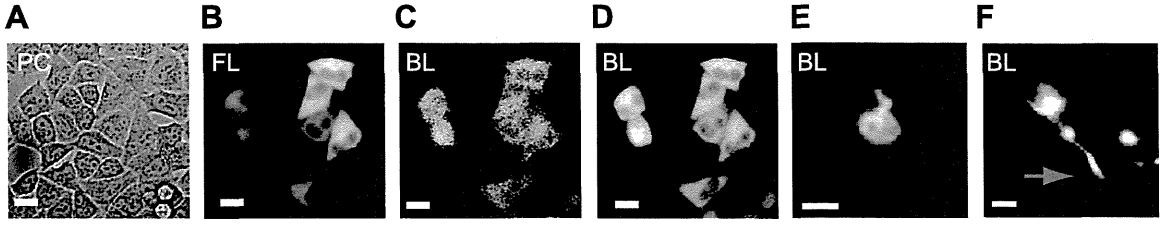

Fig. 2. Bioluminescence imaging of *ff*Luc-cp156 at the single-cell level. (A–D) Bioluminescence images of *ff*Luc-cp156 expressing HeLa cells. Images were acquired using an inverted microscope (Olympus IX71) (A, phase contrast image; B, fluorescence image; C, bioluminescence image with 500 ms camera exposure; D, bioluminescence image with 5 s camera exposure). (E and F) Bioluminescence images of a cultured microglial cell (E) and neuronal growth cones (F, red arrow). Images were acquired with 30 s camera exposure. Scale bars, 10 μm. (For interpretation of the references to color in this figure legend, the reader is referred to the web version of this article.)

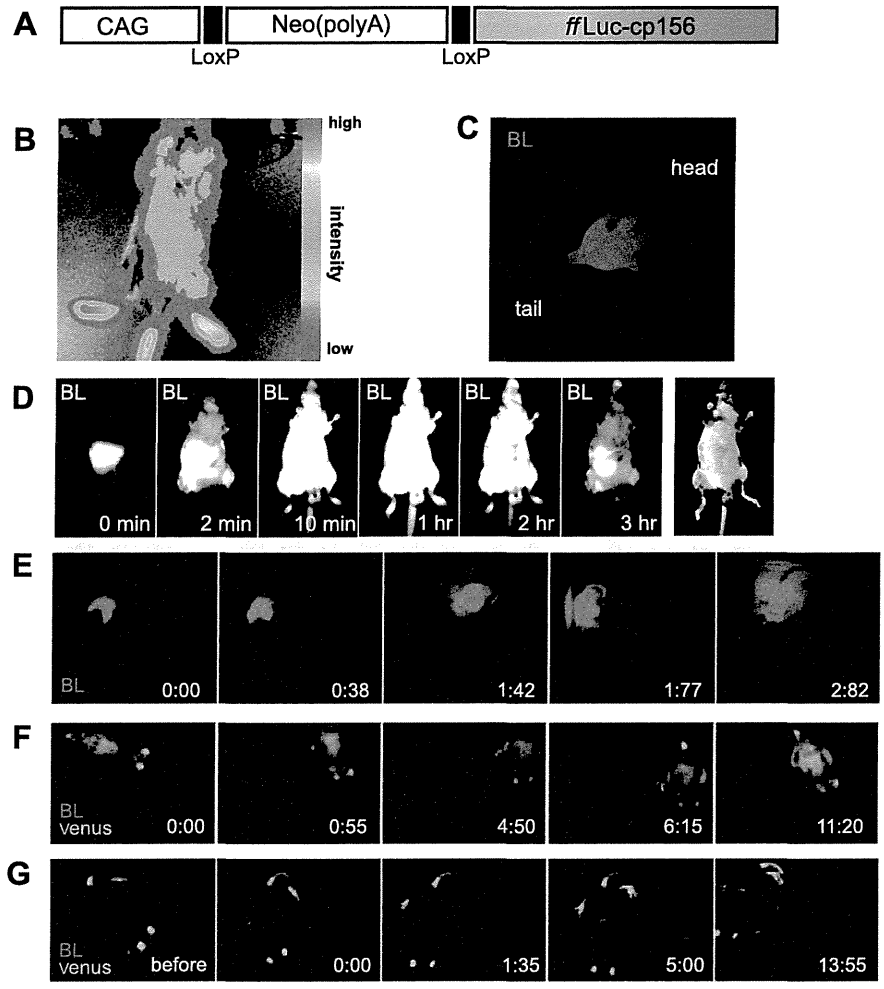

Fig. 3. Bioluminescence imaging using the *ff*Luc-cp156 transgenic mice. (A) Transgene of the *ff*Luc-cp156 reporter. (B–D) Bioluminescence images of anesthetized CAG-*ff*Luc-cp156 transgenic adult mice. (B and C) Luciferin was administered intraperitoneally. Images were acquired using the IVIS system (B) and a common digital camera (C). (D) Bioluminescence images of an anesthetized CAG-*ff*Luc-cp156 transgenic mouse that was given luciferin orally. BL, bioluminescence; FL, fluorescence. *left-most*, fluorescence image. (E–G) Bioluminescence images of freely moving CAG-*ff*Luc-cp156 transgenic adult mice acquired using an *in vivo* imaging system (LumazoneFA, Roper Japan). Bioluminescent signals are shown in red. (E) Intraperitoneal administration. Images were acquired at video rate (every 33 ms); see also Supplementary Movie 4. (F) Voluntary oral administration. Camera exposure times for bioluminescence (red) and Venus fluorescence (green) were 500 and 100 ms, respectively; see also Supplementary Movie 5. (G) Percutaneous administration. Camera exposure times for bioluminescence (red) and Venus fluorescence (green) were 1 s and 100 ms, respectively; see also Supplementary Movie 6. (For interpretation of the references to color in this figure legend, the reader is referred to the web version of this article.)

exception of spleen and red blood cells (Supplementary Fig. S2 online).

We examined the bioluminescence from an anesthetized CAG-*ff*Luc-cp156 transgenic mouse (5 months old) in the dark box of an IVIS system (Xenogen). Within 1 s after administration of luciferin (150 mg/kg BW) through the tail vein, extremely strong bioluminescence arose throughout the body, lasting for >6 h. Even with the shortest exposure time of the system (500 ms), the bioluminescent intensity exceeded the camera's saturation level. Next, we performed intraperitoneal administration of luciferin (150 mg/kg) on another anesthetized mouse (5 months old). Although rapid and strong bioluminescence developed, we acquired a bioluminescence image within the working range of the system by placing the mouse as far as possible from the objective (Fig. 3B). Bioluminescence was visible to the dark-adapted naked eye, and the image could be acquired using an ordinary digital camera (E-330, Olympus) (Fig. 3C). Considering the imaging parameters of IVIS system described in previous reports, these observations suggested that the overall bioluminescence of the CAG-*ff*Luc-cp156 transgenic mouse was over three orders of magnitude brighter than that of transgenic mice that expressed firefly luciferase (fLuc) under the control of the promoter/enhancer of the major immediate-early gene of the human cytomegalovirus (CMV-Luc) [14].

We also monitored the development of bioluminescence after oral administration of luciferin to an anesthetized mouse. As soon as a luciferin solution was injected into the mouth, strong bioluminescence was observed from the stomach (Fig. 3D, 0 min). Initially (<3 min), the stomach and intestine emitted stronger luminescence than other body parts (Fig. 3D, 2 min). Subsequently, other tissues in the trunk and limbs gradually became bioluminescent (Fig. 3D, 10 min). The spatiotemporal patterns of the spreading bioluminescence are shown in Supplementary Movie 3 online. After reaching saturation levels, these bioluminescent signals were detectable for about 6 h.

3.4. Bioluminescence imaging of freely moving CAG-ffLuc-cp156 transgenic mice

Next, we performed bioluminescence imaging experiments using awake mice. We used the *in vivo* imaging system (LumazoneFA, Roper Japan), which allowed much shorter camera